Syp1 regulates the clathrin-mediated and clathrin-independent endocytosis of multiple cargo proteins through a novel sorting motif

Amanda Reider Apel[a,†,‡], Kyle Hoban[a,†], Silvia Chuartzman[b], Raffi Tonikian[c,§], Sachdev Sidhu[c], Maya Schuldiner[b], Beverly Wendland[a], and Derek Prosser[a,‖,*]

[a]Department of Biology, Johns Hopkins University, Baltimore, MD 21218; [b]Department of Molecular Genetics, Weizmann Institute of Science, Rehovot 7610001, Israel; [c]Donnelly Centre, University of Toronto, Toronto, ON M5S 3E1, Canada

ABSTRACT **Internalization of proteins from the plasma membrane (PM) allows for cell-surface composition regulation, signaling of network modulation, and nutrient uptake. Clathrin-mediated endocytosis (CME) is a major internalization route for PM proteins. During CME, endocytic adaptor proteins bind cargoes at the cell surface and link them to the PM and clathrin coat. Muniscins are a conserved family of endocytic adaptors, including Syp1 in budding yeast and its mammalian orthologue, FCHo1. These adaptors bind cargo via a C-terminal μ-homology domain (μHD); however, few cargoes exhibiting muniscin-dependent endocytosis have been identified, and the sorting sequence recognized by the μHD is unknown. To reveal Syp1 cargo-sorting motifs, we performed a phage display screen and used biochemical methods to demonstrate that the Syp1 μHD binds DxY motifs in the previously identified Syp1 cargo Mid2 and the v-SNARE Snc1. We also executed an unbiased visual screen, which identified the peptide transporter Ptr2 and the ammonium permease Mep3 as Syp1 cargoes containing DxY motifs. Finally, we determined that, in addition to regulating cargo entry through CME, Syp1 can promote internalization of Ptr2 through a recently identified clathrin-independent endocytic pathway that requires the Rho1 GTPase. These findings elucidate the mechanism of Syp1 cargo recognition and its role in trafficking.**

Monitoring Editor
Anne Spang
University of Basel

Received: Oct 23, 2015
Revised: Jun 21, 2017
Accepted: Jun 27, 2017

INTRODUCTION

The plasma membrane (PM) of eukaryotic cells forms an essential barrier that selectively separates the fluctuating extracellular environment from the more stable conditions maintained in the cytoplasm. It contains transmembrane proteins that allow for the establishment of vital cellular gradients, regulation of cell-surface markers, modulation of signaling networks, and uptake of vital nutrients. The PM must be continuously modified in order to precisely regulate these events and accommodate the changing needs of a cell.

Clathrin-mediated endocytosis (CME) is a key pathway for modulating the composition of the PM, and this endocytic mechanism requires the action of many cytosolic proteins to internalize a portion of the membrane by generating a clathrin-coated vesicle (CCV). CCV generation requires the ordered assembly of a large number of proteins that act in discrete steps: 1) initiation of CME, in which early-arriving proteins select the endocytic site, concentrate cargo, and facilitate clathrin coat assembly; 2) maturation of the endocytic site, during which F-actin assembly and the clathrin coat promote vesicle budding; and 3) scission, in which the bud neck constricts, and the nascent vesicle is separated from the plasma membrane (Kaksonen *et al.*, 2003, 2005).

The CME machinery is largely conserved from yeast to humans, such that orthologous proteins perform equivalent functions and are recruited in a similar order (Engqvist-Goldstein and Drubin, 2003;

This article was published online ahead of print in MBoC in Press (http://www.molbiolcell.org/cgi/doi/10.1091/mbc.E15-10-0731) on July 12, 2017.

†These are co–first authors, listed alphabetically.

Present addresses: ‡Joint BioEnergy Institute, Berkeley, CA 94720; §Merck, Kenilworth, NJ 07033; ‖Department of Biology, Virginia Commonwealth University, Richmond, VA 23284.

*Address correspondence to: Derek Prosser (dprosser@vcu.edu).

Abbreviations used: CIE, clathrin-independent endocytosis; CME, clathrin-mediated endocytosis; μHD, μ-homology domain; PM, plasma membrane.

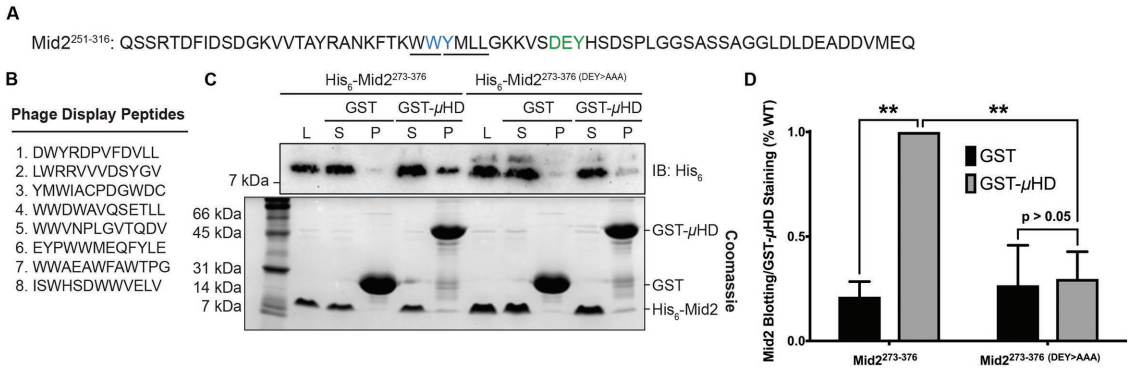

FIGURE 1: The Syp1 μHD binds a DxY motif within Mid2. (A) Amino acid sequence of Mid2$^{251-316}$. The DxY and WY motifs are shown in green and blue, respectively, and the WW and YxxΦ motifs overlapping the WY motif are underlined. (B) Amino acid sequence of the eight 12-mer peptides identified in the Syp1 μHD phage display screen. (C) Immunoblot of recombinant binding assay in which WT and mutant His$_6$-Mid2$^{273-376}$ (DEY>AAA) fragments were tested for binding to an immobilized GST-negative control or GST-Syp1 μHD; top: anti-His$_6$ immunoblot; bottom: GelCode Blue (Coomassie) protein stain. L, loading control; P, pelleted fraction; S, supernatant. (D) Quantification of Mid2 WT and mutant fragment blotting relative to staining of GST or GST-μHD recovered from pelleted fractions. Error bars indicate mean ± SD; $n = 3$; $^{**}p < 0.01$ compared with normalized WT.

Taylor *et al.*, 2011; Goode *et al.*, 2015). Adaptor proteins select specific membrane-associated cargoes for trafficking into the cell through physical interactions and are among the first components to act in CME, subsequently recruiting later-arriving components of the endocytic machinery, including clathrin.

The muniscins are a recently identified family of endocytic adaptors that includes the budding yeast protein Syp1 and its mammalian orthologues, FCHo1/2 and SGIP1 (Reider *et al.*, 2009). The muniscins have known roles in CME and are recruited to nascent sites for this pathway (Boettner *et al.*, 2009; Reider *et al.*, 2009; Henne *et al.*, 2010); however, whether muniscin-dependent cargo internalization occurs exclusively via CME has not been determined.

Muniscins mediate cargo selection via a C-terminal μ-homology domain (μHD), named for its structural similarity to the cargo-binding *μ2* subunit of the heterotetrameric AP-2 adaptor complex (Reider *et al.*, 2009). *SYP1* overexpression causes partial relocalization of Mid2 to the vacuole in a μHD-dependent manner (Reider *et al.*, 2009), whereas the FCHo1 μHD interacts with the BMP receptor Alk8 (Umasankar *et al.*, 2012). Of note, the yeast orthologue of *μ2*, known as Apm4, can also bind to Mid2 and affect its localization (Chapa-y-Lazo *et al.*, 2014). The mechanism by which muniscins recognize their cognate cargo proteins is unclear.

Most endocytic adaptors contain one or more regions that bind short, linear peptide sequences known as cargo-sorting motifs, which are present in the cytoplasmic regions of their transmembrane cargoes (Reider and Wendland, 2011). The wide variety of PM-localized cargoes necessitates the use of several different sorting motifs to prevent competition for entry into the cell, as well as to allow for maximal flexibility and regulation of specific cargo internalization. Numerous sorting motifs have been identified, each of which has a distinct amino acid sequence (Traub, 2009).

AP-2 binds two different cargo-sorting motifs: YxxΦ (where Φ is any amino acid with a bulky, hydrophobic side chain) through the *μ2* subunit, and [D/E]xxxL[L/I/M] motifs through the σ2 subunit (Boll *et al.*, 1996; Owen *et al.*, 2004; Doray *et al.*, 2007; Kelly *et al.*, 2008). Other adaptor proteins that contain variant phosphotyrosine-binding domains, such as Dab2, ARH, and talin, bind to nonphosphorylated [F/Y]XNPXxNPx[Y/F] sorting motifs found in the tails of membrane cargoes such as integrins and the low-density lipoprotein receptor (Keyel *et al.*, 2006; Wegener *et al.*, 2007). The yeast-specific adaptor protein Sla1 interacts with NPFxD sorting motifs within its cargoes, Ste2 and Wsc1, through its Sla1-homology domain 1 region (Howard *et al.*, 2002; Piao *et al.*, 2007). Other cargoes lack any known sorting sequences, leading to the prediction that additional motifs have yet to be determined.

The only known Syp1 cargo is the cell wall stress sensor Mid2 (Reider *et al.*, 2009). The smallest fragment of Mid2 demonstrated to bind the Syp1 μHD is Mid2$^{251-316}$ (Reider *et al.*, 2009; Figure 1A), suggesting that the sorting motif recognized by Syp1 resides in this region of the cargo. Intriguingly, Mid2 is a component of a clathrin-independent endocytosis (CIE) pathway in yeast, which requires the Rho1 GTPase and its effector, the formin Bni1 (Prosser *et al.*, 2011); however, a potential role for Syp1 in cargo trafficking via CIE has not yet been addressed. This is due, in part, to the fact that Mid2 localizes primarily to the PM and requires *SYP1* overexpression for observable trafficking into the cell (Reider *et al.*, 2009), complicating the use of Mid2 in live-cell studies of Syp1-mediated endocytosis.

Identifying additional cargoes that localize to downstream endocytic compartments would aid in examining the potential involvement of Syp1 in both endocytic pathways under standard conditions and in testing the role for a potential cargo-sorting motif in vivo. To improve our understanding of the molecular mechanisms underlying muniscin-mediated cargo trafficking, we sought to identify cargo-sorting motifs recognized by the Syp1 μHD. Using a phage display screen, we demonstrated that DxY is a cargo-sorting motif; moreover, visual screening revealed the peptide transporter Ptr2 and ammonium permease Mep3 as Syp1 cargoes. Finally, we identified a role for Syp1 in clathrin-independent endocytosis of Ptr2, suggesting that Syp1 participates in multiple endocytic pathways.

RESULTS

The Syp1 μHD binds a DxY motif within Mid2

To reveal peptide sequences bound by the Syp1 μHD, we performed an unbiased phage display screen using a random 12-mer peptide library. The μHD was tagged with glutathione *S*-transferase (GST), expressed in bacteria, purified, and used as a target in binding selections with the phage display library. From the screen, we identified eight potential Syp1 ligand sequences and, to aid in the search for potential motifs, we compared the peptide sequences to

that of Mid2$^{251-316}$, the smallest fragment of Mid2 previously shown to bind the Syp1 μHD (Figure 1, A and B; Reider *et al.*, 2009). Two DxY sequences (peptides 1 and 2), two YxxΦ motifs (peptides 3 and 6), and several instances of two consecutive residues with bulky side chains, including one WY (peptide 1) and five WW sequences (peptides 4–8), were present in the peptides. All of these potential Syp1-interacting motifs are present in Mid2$^{251-316}$.

Due to the abundance of consecutive, bulky side chains in our phage display results, we initially sought to investigate the role of this candidate motif in cargo binding by Syp1. The WY motif overlaps with both a WW and a YxxΦ motif (276-WWYMLL; Figure 1A); therefore, we generated a mutant in which the WY residues were mutated to alanines to allow for the simultaneous disruption and investigation of all three motifs. We examined binding of the μHD to the WY>AA mutant protein using an affinity pull-down experiment. For these tests, a longer Mid2 fragment, Mid2$^{273-376}$, was used as a result of its increased amenability for use in biochemical assays. Mutation of the WY sequence (amino acids [aa] 277–278) did not have an observable effect on binding of hexahistidine (His_6)-tagged Mid2$^{273-376}$ to the Syp1 μHD; similar amounts of the wild-type (WT) and mutant protein were recovered in the bead fraction when coprecipitated with GST-μHD (Supplemental Figure S1A). Consequently, these data indicate that the WW and WY (WW/Y) motifs, along with the YxxΦ motif, in the Mid2 C-terminal tail are unlikely to bind Syp1.

On the basis of our results indicating that these motifs are not required for Syp1 binding to Mid2, we tested the ability of the μHD to bind the DxY motif. The residues DEY (aa 287–289) were mutated to alanines, and affinity pull-down experiments using His_6-Mid2$^{273-376}$ and GST-μHD revealed that, whereas the WT protein bound to the μHD as expected, mutation of the DxY motif significantly reduced the amount of Mid2 that coprecipitated with GST-μHD (Figure 1, C and D). Together, these results demonstrate that the Syp1 μHD binds the DxY motif in its known cargo protein, Mid2.

Syp1 also recognizes a DxY motif within Snc1

A previous high-throughput study demonstrated that the vesicle–soluble *N*-ethylmaleimide–sensitive factor (NSF) attachment protein receptor (v-SNARE) Snc1 exhibits a decreased rate of endocytosis in mutant strains lacking some CME-associated genes, including a modest defect in *syp1*Δ cells (Burston *et al.*, 2009). Although greater defects were observed in cells lacking other adaptor-encoding genes, cargo proteins are often trafficked into the cell by multiple adaptors. For example, in the study by Burston *et al.* (2009), deletion of either *YAP1801* or *YAP1802* individually produced a mild Snc1 endocytosis defect but, when they were removed from the genome in combination, the inhibition of Snc1 internalization was more severe.

Of note, Snc1 also contains DxY, WY, and YxxΦ motifs in its cytoplasmic domain (Figure 2A). Given that Syp1 interacts directly with Mid2 to promote its internalization, we reasoned that Syp1 might similarly associate with Snc1. Thus, we investigated a potential role for Syp1 in Snc1 endocytosis. Owing to the previous observation that only a subtle reduction in Snc1 trafficking occurs in *syp1*Δ cells (Burston *et al.*, 2009), we chose to test the effect of *SYP1* overexpression on Snc1 localization.

To assess changes in Snc1 localization, we transformed WT cells expressing green fluorescent protein (GFP)-Snc1 from a low-copy plasmid with either an empty high-copy vector or one containing *SYP1* expressed from its endogenous promoter. In cells with empty vector, GFP–Snc1 was polarized to the PM of the daughter bud in medium- to large-budded cells (Figure 2B, left; arrowheads), as expected (Robinson *et al.*, 2006). The protein also localized to internal punctae, likely due to constitutive endocytosis and recycling. In contrast, the localization of GFP-Snc1 to the PM was less pronounced in buds of similar size from cells with high-copy expression of *SYP1*. Instead, most of the protein localized to internal compartments within buds (Figure 2B, right; arrowhead). We also observed increased GFP-Snc1 internalization in unbudded cells, indicating that the effect of Syp1 on Snc1 internalization is not cell cycle dependent (Figure 2B, arrows). Overall, these data demonstrate that Syp1 can contribute to Snc1 trafficking.

Owing to the ability of Syp1 to promote Snc1 endocytosis in vivo, as well as the presence of candidate Syp1-binding motifs in the Snc1 cytoplasmic domain, we next tested whether recombinant Syp1 and Snc1 bind in vitro. The His_6-tagged cytosolic domain

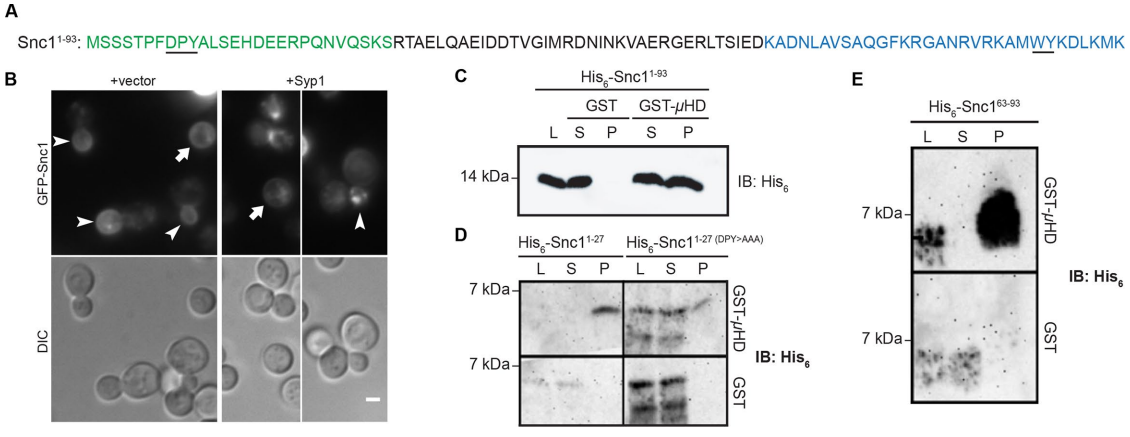

FIGURE 2: Syp1 recognizes a DxY motif within Snc1. (A) Amino acid sequence of the cytoplasmic region of Snc1, aa 1–93. Snc1$^{1-27}$ is shown in green and Snc1$^{63-93}$ in blue; the DxY and WY motifs are underlined. (B) WT cells expressing GFP-Snc1 from a low-copy plasmid were transformed with either an empty or *SYP1*-containing high-copy vector and grown on selective medium. Cells were imaged via live-cell fluorescence microscopy (arrowheads: GFP-Snc1 in medium- to large-sized buds; arrows: GFP-Snc1 in unbudded cells). Scale bar, 2 μm. (C) Immunoblot of binding assay in which GST and GST-Syp1 μHD were treated with WT His_6-Snc1$^{1-93}$. L, loading control; P, pelleted fraction; S, supernatant. (D) Immunoblot of binding assay in which WT His_6-Snc1$^{1-27}$ and a mutant of this fragment (DPY>AAA) were tested for binding to the Syp1 μHD. L, loading control; P, pelleted fraction; S, supernatant. (E) Immunoblot of binding assay in which Snc1$^{63-93}$ was tested for binding to GST-Syp1 μHD. L, loading control; P, pelleted fraction; S, supernatant.

of Snc1 (aa 1–93) bound to GST-μHD but not to GST alone, confirming Snc1 as a binding partner of Syp1 (Figure 2C). To determine whether the DxY motif near the N-terminus of Snc1 binds to Syp1 as did the DxY motif of Mid2, we tested a His_6-tagged fragment of Snc1 containing this motif, $Snc1^{1-27}$ (Figure 2A, green), for binding to the μHD. $Snc1^{1-27}$ bound the μHD, indicating that this region physically interacts with Syp1 (Figure 2D). Moreover, binding was reduced when the DxY motif in this fragment was mutated to alanines, suggesting that the DxY motif may be a common sorting sequence among Syp1 cargoes.

Although the DxY motif is necessary for binding to the Syp1 μHD in the context of $Snc1^{1-27}$, results of an experiment using a longer fragment of Snc1 (aa 1–93) indicated that this cargo contains more than one Syp1-binding site. $Snc1^{1-93}$ still interacted with Syp1 when the DxY motif in this fragment was mutated; even charge reversal of the aspartic acid to lysine did not abrogate the interaction (Supplemental Figure S1B). As a result, additional fragments of the Snc1 cytoplasmic tail were constructed and tested for binding to the Syp1 μHD. The last third of the Snc1 tail (aa 63–93; Figure 2A, blue) also bound to the μHD (Figure 2E).

$Snc1^{63-93}$ does not contain a DxY motif but does have WY and YxxΦ motifs, both of which were present in the phage display peptides. Therefore we tested the ability of Syp1 to bind these motifs in the $Snc1^{63-93}$ fragment. Mutation of the WY residues (aa 86–87) to alanines, which simultaneously disrupts the WY and YxxΦ motifs, did not inhibit binding of $Snc1^{63-93}$ to the μHD (Supplemental Figure S1C). Along with results of the Mid2 WY mutant–binding experiment, this further suggests that Syp1 does not bind WY motifs in these cargoes; the precise nature of association between Syp1 and $Snc1^{63-93}$ will be a subject of future study. Together, these findings indicate that Snc1 contains at least two Syp1-binding sites, including a DxY motif, both of which are independent of the previously identified Snc1 endocytic signal V40, M43 within $Snc1^{28-62}$ (Gurunathan *et al.*, 2000; Burston *et al.*, 2009).

A visual screen reveals Ptr2 and Mep3 to be Syp1 cargoes

Given that Syp1 and its mammalian orthologues play conserved roles as adaptor proteins, we hypothesized that Syp1 might regulate endocytosis of cargoes other than Mid2 and Snc1. Because short peptide motifs such as DxY are likely to be found in many proteins, we attempted to identify potential Syp1-dependent cargoes using an unbiased, high-throughput visual screen in order to improve our understanding of the cellular roles for this adaptor.

To establish that deletion of *SYP1* does not impair trafficking of all endocytic cargoes, we first examined the localization of GFP-tagged Ste3 in WT and *syp1*Δ cells. Ste3, the yeast **a**-factor mating pheromone receptor, is constitutively endocytosed in nonmating *MAT*α cells and localizes primarily to the vacuole (Davis *et al.*, 1993). Ste3-GFP internalization was not disrupted in a *syp1*Δ strain, with protein localization appearing similar to that in WT cells (Figure 3A). In contrast, the absence of End3, a key endocytic protein that acts in coordination with the accessory proteins Sla1 and Pan1 (Tang *et al.*, 1997, 2000), causes cargoes, including Ste3, to nonspecifically accumulate at the plasma membrane (Raths *et al.*, 1993).

To quantify the amount of Ste3 at the PM in each condition, we also constructed a chimera using pHluorin (Figure 3B), a pH-sensitive variant of GFP that allows for analysis of endocytic efficiency (Miesenbock *et al.*, 1998; Prosser *et al.*, 2010). Quantification of Ste3-pHluorin intensity corroborated the results obtained from Ste3-GFP imaging: the *syp1*Δ mutants did not exhibit increased Ste3-pHluorin fluorescence, unlike the significant increase observed in the *end3*Δ strain. These data suggest that loss of Syp1 does not generally interrupt endocytosis of cargo and might instead affect the internalization of specific proteins. Therefore, a *syp1*Δ strain was used in our visual screen to identify novel Syp1 cargoes.

Using the commercially available Yeast GFP Library, which expresses C-terminally

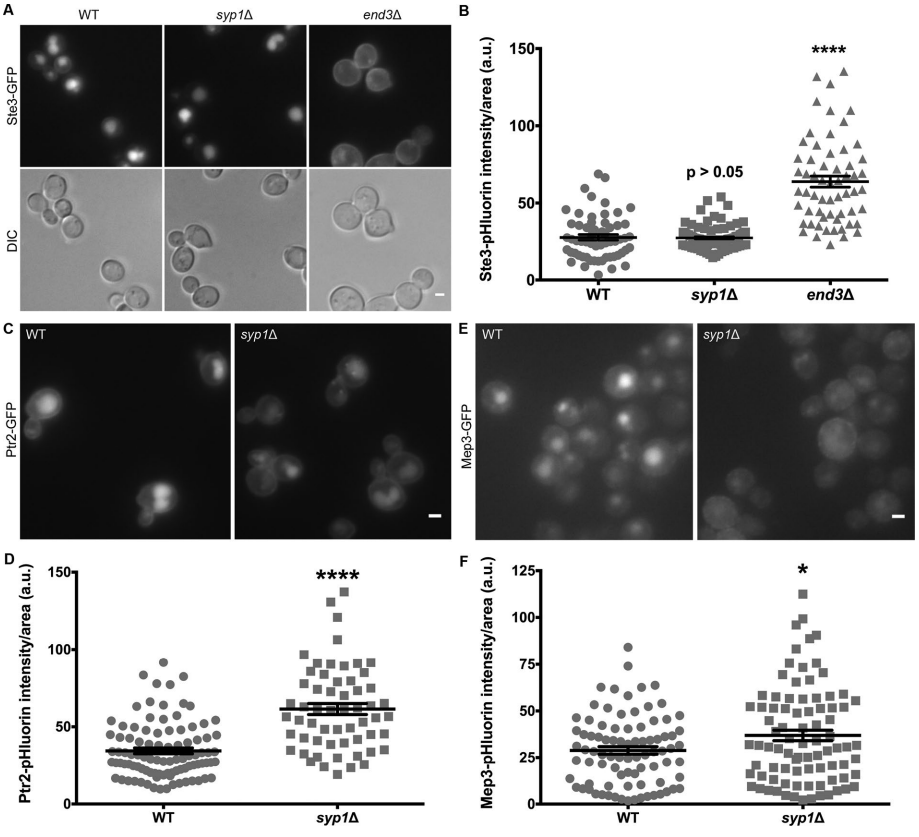

FIGURE 3: A visual screen reveals Ptr2 and Mep3 to be Syp1 cargoes. (A) WT, *syp1*Δ, and *end3*Δ cells expressing Ste3-GFP were grown on rich medium and imaged via live-cell fluorescence microscopy. Scale bar, 2 μm. (B) Intensity of Ste3-pHluorin was quantified for each condition; intensity values were corrected for cell size and expressed in arbitrary units (a.u.). Error bars indicate mean ± SEM; ****$p < 0.0001$ compared with WT. (C) WT and *syp1*Δ cells expressing Ptr2-GFP were grown on rich medium (YPD) and imaged via live-cell fluorescence microscopy. Scale bar, 2 μm. (D) Intensity of Ptr2-pHluorin was quantified for each condition; intensity values were corrected for cell size and expressed in arbitrary units (a.u.). Error bars indicate mean ± SEM; ****$p < 0.0001$ compared with WT. (E) WT and *syp1*Δ cells expressing Mep3-GFP were grown on minimal, ammonium-rich medium (YNB) and imaged via live-cell fluorescence microscopy. Scale bar, 2 μm. (F) Intensity of Mep3-pHluorin was quantified for each condition; intensity values were corrected for cell size and expressed in arbitrary units (a.u.). Error bars indicate mean ± SEM; *$p < 0.05$ compared with WT.

tagged genes (Huh *et al.*, 2003), we selected the complete set of 203 proteins with at least one predicted transmembrane domain that have reported localization to one or more regions of the cell along the endocytic route: periphery, bud neck, endosomes, and vacuoles. These proteins represent the set of possible Syp1-dependent cargoes (Supplemental Table S1). Strains expressing GFP-tagged proteins were mated with *syp1*Δ cells and sporulated, and the resulting haploids were selected for *syp1*Δ mutants expressing the GFP fusion (Cohen and Schuldiner, 2011). We used live-cell fluorescence microscopy to screen for proteins with altered localization in the *syp1*Δ strain compared with WT cells.

From the screen, 10 candidate Syp1 cargoes were identified. The candidates were then reconstructed in a separate genetic background strain (W303), different from the background of the GFP Library (BY4742), to verify independently the results of the screen (Supplemental Figure S2A and Figure 3, C–F). Two proteins, Ptr2 and Mep3, continued to exhibit notably altered localization in the absence of Syp1 after reconstruction (Figure 3, C–F) and consequently were chosen for further investigation.

Ptr2 is a dipeptide/tripeptide transporter that functions at the PM and is a member of a peptide transport family of proteins conserved from archaeans to humans (Steiner *et al.*, 1994; Saier, 2000). Ptr2-GFP localized mainly to the vacuole in cells grown on rich medium, with some protein also visible at the PM (Figure 3C). However, trafficking of Ptr2-GFP to the vacuole was reduced in the *syp1*Δ strain, with more protein accumulating at the PM than in WT cells. Although it was decreased, endocytosis of Ptr2 was not abolished in *syp1*Δ cells, indicating that there are likely additional adaptor proteins that contribute to internalization of this cargo. Quantification of Ptr2-pHluorin revealed a significant increase in Ptr2 concentration at the PM of *syp1*Δ cells compared with WT (Figure 3D), in agreement with findings using GFP. These results suggest that Ptr2 is a novel Syp1 cargo.

The other candidate Syp1 cargo that we chose to investigate further was the ammonium permease Mep3 (Marini *et al.*, 1997). Ammonium-transporting Mep proteins in budding yeast share sequence homology to the Rhesus family of mammalian proteins (Heitman and Agre, 2000). Mep3-GFP localized primarily to the vacuole in a WT background when cells were grown on minimal, ammonium-rich medium; however, with the loss of Syp1, internalization of the protein was reduced, and cells exhibited decreased fluorescent signal at the vacuole (Figure 3E). Quantification of a Mep3-pHluorin chimera indicated that its concentration at the PM was significantly increased in a *syp1*Δ strain compared with WT cells (Figure 3F). This implies that Syp1 also selectively recognizes Mep3 for trafficking into the cell. Although decreased, Mep3 endocytosis continued in the absence of Syp1, suggesting that Mep3, like Ptr2, is also selected for internalization by other factors in addition to Syp1.

To rule out the possibility that differences observed in *syp1*Δ cells may not result from a loss of Syp1 function at the PM but instead are a result of inhibiting direct Golgi-to-vacuole trafficking of cargoes, we treated strains expressing fluorescently tagged cargoes with latrunculin A (LatA). LatA inhibits the polymerization of F-actin, causing a complete block in endocytosis, but does not impair Golgi-to-vacuole transport (Ayscough *et al.*, 1997; Huang and Chang, 2011). When treated with LatA, WT cells showed a significant increase in the amount of Ptr2 and Mep3 at the PM compared with controls (Supplemental Figure S3, A and B), indicating that contributions of Syp1 to the localization of these cargoes are indeed due to its function at the PM.

DxY motifs mediate Syp1-dependent trafficking in vivo

All 10 candidate Syp1 cargoes possess either a DxY motif or biochemically similar sequence, such as DxΦ or ExY. For 8 of the candidates, the motifs reside in a region of the cargo predicted to be in the cytoplasm upon analysis using the topology prediction program SPOCTOPUS (Viklund *et al.*, 2008), specifically including several DxY motifs (Supplemental Figure S2B and Figure 4A). Of note, the two validated cargoes, Mep3 and Ptr2, contain a DxY motif, suggesting that Syp1 may promote endocytosis of an expanded list of cargoes with this sorting sequence.

The Ptr2 DxY motif (aa 35–37) falls within an N-terminal region previously predicted to reside in the cytoplasm (Hauser *et al.*, 2005). The topology of Mep3, however, is unknown. The result of the SPOCTOPUS projection for Mep3 places the DxY sequence within a C-terminal, cytoplasmic tail (Figure 4A). Based on predicted topology, DxY motifs in the cytoplasmic regions of Ptr2 and Mep3 would be accessible for binding to the Syp1 μHD. The C-terminal DxY motif in Mep3 also permits short truncations of the protein to test the role of the motif in Mep3 trafficking while readily retaining the majority of the protein sequence under control of the endogenous promoter. For this reason, we chose Mep3 over Ptr2 for further in vivo studies examining DxY motifs.

We previously demonstrated that the Syp1 μHD is specifically responsible for binding to and internalizing Mid2 (Reider *et al.*, 2009). To demonstrate that this is true for Syp1 internalization of Mep3, we introduced full-length *SYP1* on a high-copy plasmid, as well as a truncated form in which the μHD is absent, into *syp1*Δ cells expressing genomically encoded Mep3-GFP. Therefore the plasmid-borne *SYP1* was the sole source of Syp1 protein in this experiment. As expected, high-copy expression of full-length *SYP1* rescued Mep3 internalization and significantly decreased the amount of Mep3-GFP or Mep3-pHluorin at the PM below WT levels (Figure 4, B and C). However, high-copy expression of truncated Syp1 lacking the μHD did not rescue the endocytic defect. Instead, Mep3-GFP remained primarily at the PM, comparable to the *syp1*Δ strain with empty vector. This result demonstrates that Mep3 behaves similarly to the previously identified cargo Mid2 and suggests that the Syp1 μHD is required for internalization of both cargoes.

We next used a truncation approach to assess the role of the DxY motif in Mep3 trafficking. When Mep3 was truncated in an otherwise WT background by placing a fluorescent tag just N-terminal to its DxY motif (aa 431–433), thereby removing the sorting signal and all downstream residues, the truncated Mep3$^{\Delta 430}$ protein (aa 1–430) displayed significantly reduced trafficking to the vacuole and increased retention at the PM (Figure 4, D and E). The localization of Mep3$^{\Delta 430}$-GFP to the PM supports results of the topological prediction that the Mep3 DxY motif resides within a cytoplasmic region of the protein; if the DxY motif were located within an extracellular region of Mep3, the GFP tag would translocate to the endoplasmic reticulum (ER) lumen during protein synthesis, which presents a challenging environment for GFP folding in many contexts and can lead to aberrant retention in the ER (Jain *et al.*, 2001).

In addition, we constructed a Mep3 truncation, Mep3$^{\Delta 433}$ (aa 1–433), in which the DxY motif is retained but all downstream residues are replaced with a GFP tag. Imaging and results of pHluorin quantification for this truncation demonstrated that the inclusion of these three amino acids partially, yet significantly, rescued trafficking of the Mep3$^{\Delta 430}$ mutant (Figure 4, D and E). There are several possibilities as to why the rescue of Mep3 truncation endocytosis by reintroduction of the DxY motif was incomplete. For example, additional sorting signals regulating internalization of this cargo may

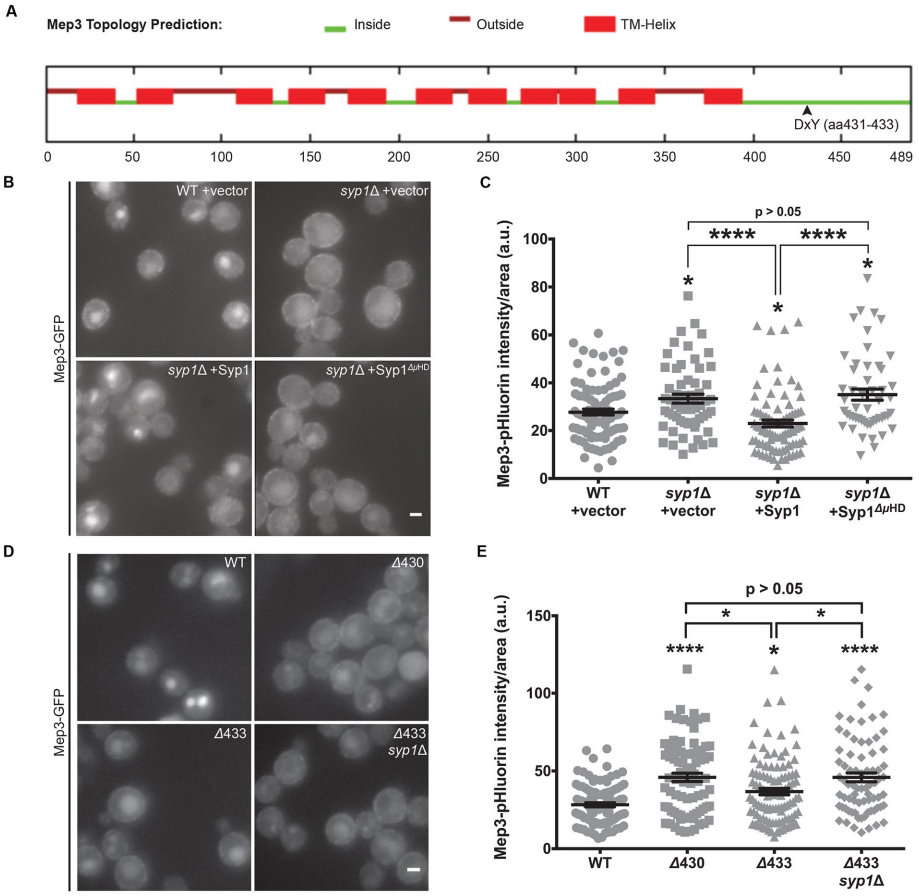

FIGURE 4: A DxY motif contributes to Mep3 trafficking. (A) Full-length Mep3 sequence was analyzed using the SPOCTOPUS membrane protein topology prediction algorithm. The DxY motif (aa 431–433) is indicated (Inside, cytoplasmic; Outside, extracellular; TM-Helix, transmembrane). (B) Localization of Mep3-GFP in WT or *syp1*Δ cells transformed with empty high-copy vector, high-copy *SYP1*, or high-copy *SYP1* lacking the μHD was examined by live-cell fluorescence microscopy. Scale bar, 2 μm. (C) Fluorescence intensity from cells expressing Mep3-pHluorin was quantified for each condition; intensity values were corrected for cell size and expressed in arbitrary units (a.u.). Error bars indicate mean ± SEM; *$p < 0.05$, ****$p < 0.0001$ compared with WT. (D) Cells expressing full-length Mep3-GFP, Mep3$^{\Delta 430}$-GFP, or Mep3$^{\Delta 433}$-GFP in WT and *syp1*Δ backgrounds were grown on minimal medium and imaged via live-cell fluorescence microscopy. Scale bar, 2 μm. (E) Intensity of Mep3-pHluorin for each condition was quantified; intensity values were corrected for cell size and expressed in arbitrary units (a.u.). Error bars indicate mean ± SEM; *$p < 0.05$, ****$p < 0.0001$ compared with WT.

be present within the sequence downstream of the DxY motif; this would not be unexpected, due to the existence of Syp1-independent mechanisms of Mep3 endocytosis (Figure 3, E and F). Deletion of *SYP1* abolished the rescue observed with reintroduction of the DxY motif, demonstrating that Syp1 is responsible for DxY-mediated rescue of Mep3 internalization in this experiment. Overall, these results indicate that a DxY motif affects Syp1 trafficking of Mep3 in vivo.

A similar experiment was performed for Mid2 in which truncations with (Mid2$^{\Delta 289}$-GFP) and without (Mid2$^{\Delta 286}$-GFP) the DxY motif were tested for internalization in cells expressing high-copy *SYP1* (Supplemental Figure S1D). Results regarding the role of the DxY motif in Mid2 trafficking were inconclusive; many cells expressing Mid2$^{\Delta 289}$-GFP, which includes the DxY motif, failed to induce trafficking of this Mid2 truncation to the vacuole. This highlights the usefulness of the alternative cargoes identified in the visual screen. However, we observed that Mid2$^{\Delta 286}$-GFP, which lacks the DxY motif and downstream C-terminus but retains the Mid2 WW/Y and YxxΦ motifs, exhibited decreased internalization even in the presence of high-copy Syp1, supporting the conclusion that these sequences do not contribute to Mid2 recognition by Syp1.

Ammonium-induced trafficking of Mep3 is interrupted in *syp1*Δ cells

In our examinations of Mep3-GFP localization, we observed that the localization of this protein is sensitive to changes in growth medium. Mep3 remained primarily at the PM during growth in nutrient-rich conditions but localized mainly to the vacuole on minimal, ammonium-rich medium. In yeast, many nutrient permeases are internalized under conditions of high extracellular ligand concentrations (Conrad *et al.*, 2014); thus, we tested whether Mep3 internalization could be induced in response to ammonium. In an attempt to observe Mep3-GFP trafficking over time, we grew cells in rich conditions with a low ammonium concentration and shifted them to minimal medium with high levels of ammonium.

Unlike cells grown continuously in low-ammonium (rich) conditions, those grown in high-ammonium (minimal) medium displayed trafficking of Mep3-GFP to the vacuole after 4 h (Supplemental Figure S4A). pHluorin quantification was precluded because the time course was longer than a cell division cycle (Prosser *et al.*, 2016), raising concern for dilution of pHluorin-tagged protein upon formation of daughter cells. However, Mep3-GFP remained almost entirely at the PM of cells grown in rich medium, in contrast to the internalization observed in response to ammonium.

To determine whether trafficking of Mep3 in response to high ammonium concentration requires Syp1, we performed an experiment in which both WT and *syp1*Δ cells grown in rich conditions were treated with minimal, high-ammonium medium (Figure 5A). We quantified trafficking by categorizing cells as having strong, moderate, or weak/absent localization of Mep3-GFP to the vacuole (Figure 5B). The two strains displayed a similar predominance of Mep3-GFP at the PM at the start of the time course (0 h), with no obvious differences between WT and *syp1*Δ cells. Conversely, at 4 h after shift to ammonium-rich medium, the WT strain exhibited greater trafficking of Mep3-GFP into the cell than the *syp1*Δ strain for all three localization classes. These results indicate that the ammonium-induced internalization of Mep3-GFP is Syp1-dependent.

We hypothesized that altered Mep3 trafficking under different growth conditions might result from changes in the expression of Syp1 or amount of Syp1 at sites of CME. To examine this possibility, we grew cells expressing Syp1-GFP in either rich or minimal, high-ammonium medium. The intensity of Syp1-GFP punctae at the PM appeared brighter in cells grown on minimal medium than with rich medium (Figure 5C). This condition-dependent change in

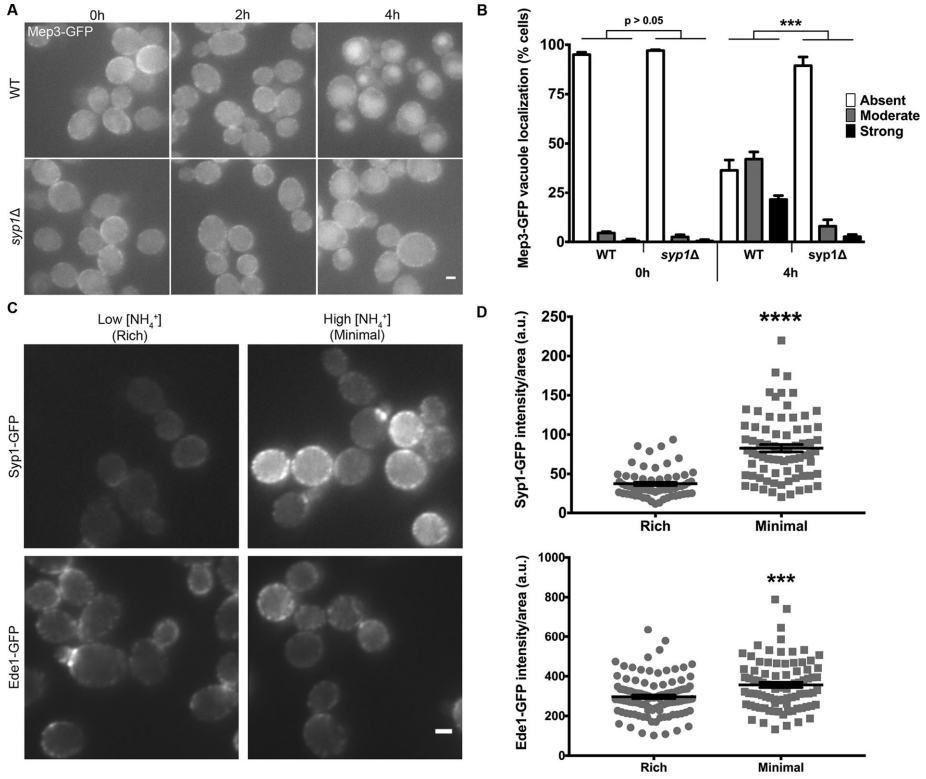

FIGURE 5: Ammonium-induced trafficking of Mep3 is interrupted in *syp1*Δ cells. (A) WT and *syp1*Δ cells were grown to mid-logarithmic phase in rich medium (YPD) and then resuspended in minimal medium (YNB). Cells were imaged every 2 h via live-cell fluorescence microscopy. Scale bar, 2 μm. (B) WT and *syp1*Δ cells at 0 and 4 h after shift to high ammonium medium were categorized as having strong, moderate, or weak/absent localization of Mep3-GFP to the vacuole (black, gray, and white bars, respectively; ***$p < 0.001$; each mutant phenotypic class per time point was compared with its respective WT class of the same time point). (C) Cells expressing Syp1-GFP and Ede1-GFP were grown on either rich medium or high ammonium-containing minimal medium and imaged via live-cell fluorescence microscopy. Scale bar, 2 μm. (D) Intensity of Syp1- or Ede1-GFP fluorescence per cell was quantified for each condition; intensity values were corrected for cell size and expressed in arbitrary units (a.u.). Error bars indicate mean ± SEM; ***$p < 0.001$, ****$p < 0.0001$ compared with WT).

fluorescence was greater for Syp1-GFP than Ede1-GFP, which, along with Syp1, is the earliest-arriving protein to nascent CME events in yeast.

Quantification of cells expressing each chimeric protein demonstrated that the fluorescence intensity of Syp1- and Ede1-GFP increased on minimal medium; however, the enhancement was greater for Syp1 than for Ede1 (Figure 5D). These data indicate that, although the earliest-arriving CME factors appear to exhibit generally increased levels at endocytic sites in cells grown with minimal medium, the intensity of Syp1 fluorescence is elevated to a greater extent under these conditions.

To determine whether the increased Syp1-GFP intensity during growth on minimal medium is due to an altered level of Syp1 expression as opposed to changes in recruitment to endocytic sites, we examined the total amount of Syp1-GFP in cells grown in rich and minimal media. Immunoblotting against Syp1-GFP with anti-GFP antibodies demonstrated that growth on rich medium did not decrease cellular levels of Syp1 (Supplemental Figure S4B). Together, these data suggest that enhanced Syp1-mediated trafficking of Mep3 in cells exposed to high levels of ammonium is due to increased concentration of Syp1 at sites of CME.

Ptr2 can be trafficked via Rho1-mediated clathrin-independent endocytosis

Previous studies established that Syp1 and its homologue, FCHo1, are involved in the initiation and regulation of CME and that Syp1 acts as an adaptor to internalize cargo (Boettner *et al.*, 2009; Reider *et al.*, 2009; Stimpson *et al.*, 2009; Henne *et al.*, 2010). However, an exclusive role for Syp1 in clathrin-mediated cargo internalization has not been demonstrated. Of note, the Syp1 cargo, Mid2, plays a role in activation of Rho1-mediated CIE (Prosser *et al.*, 2011), suggesting that Syp1 may have additional functions in cargo trafficking via CIE.

To evaluate the role of CME in Syp1-mediated internalization, we tagged cargoes in *end3*Δ strains in which CME is disrupted. We first tested the ability of high-copy Syp1 to promote internalization of Mid2 from PM to vacuole in *end3*Δ cells. As expected, high-copy expression of *SYP1* in WT cells increased trafficking of Mid2 to the vacuole (Reider *et al.*, 2009; Supplemental Figure S5A), whereas Syp1-dependent internalization was blocked in *end3*Δ cells, suggesting that Mid2 is a CME-specific cargo despite its role in activating Rho1-dependent CIE. Similarly, the results of an experiment with Snc1, in which the internalization of GFP-Snc1 in cells with high-copy *SYP1* was disrupted by the loss of End3, led to the conclusion that this cargo is also trafficked predominantly via CME (Supplemental Figure S5B).

We used the same strategy for determining the role of CME in the internalization of our newly identified Syp1 cargoes, Mep3 and Ptr2. In *end3*Δ cells, both Mep3 and Ptr2 trafficking was largely blocked compared with WT, leading to their accumulation at the PM (Figure 6, A–C). These results indicate that CME contributes predominantly to the internalization of Syp1 cargoes identified by the visual screen as well. However, Ptr2 displayed continued trafficking into cells despite the CME deficiency (Figure 6A, arrows), a phenotype that was not observed for other cargoes in an *end3*Δ mutant.

To determine whether Rho1-dependent CIE may be responsible for continued Ptr2 trafficking in CME mutants, we grew cells expressing Ptr2-GFP in the presence of 1 M sorbitol, which has been shown to up-regulate CIE in yeast (Prosser *et al.*, 2011). Trafficking of Ptr2-GFP into *end3*Δ cells was improved by the addition of sorbitol to the medium (Figure 6A). In contrast, Mep3 showed only subtle improvement in endocytosis with osmotic support. This result suggests that the rescue of internalization by osmotic support is more specific to Ptr2. Unfortunately, the addition of sorbitol to the growth medium inhibits pHluorin quenching within vacuoles, barring the use of pHluorin chimeras for quantification of endocytosis (Supplemental Figure S5C; D.P., unpublished results). Thus we used the same approach of counting the proportion of cells with strong, moderate, or weak/absent vacuole fluorescence as in previous experiments. We observed that endocytosis of Ptr2-GFP in *end3*Δ cells was rescued to near WT levels by addition of sorbitol to the medium (Figure 6D).

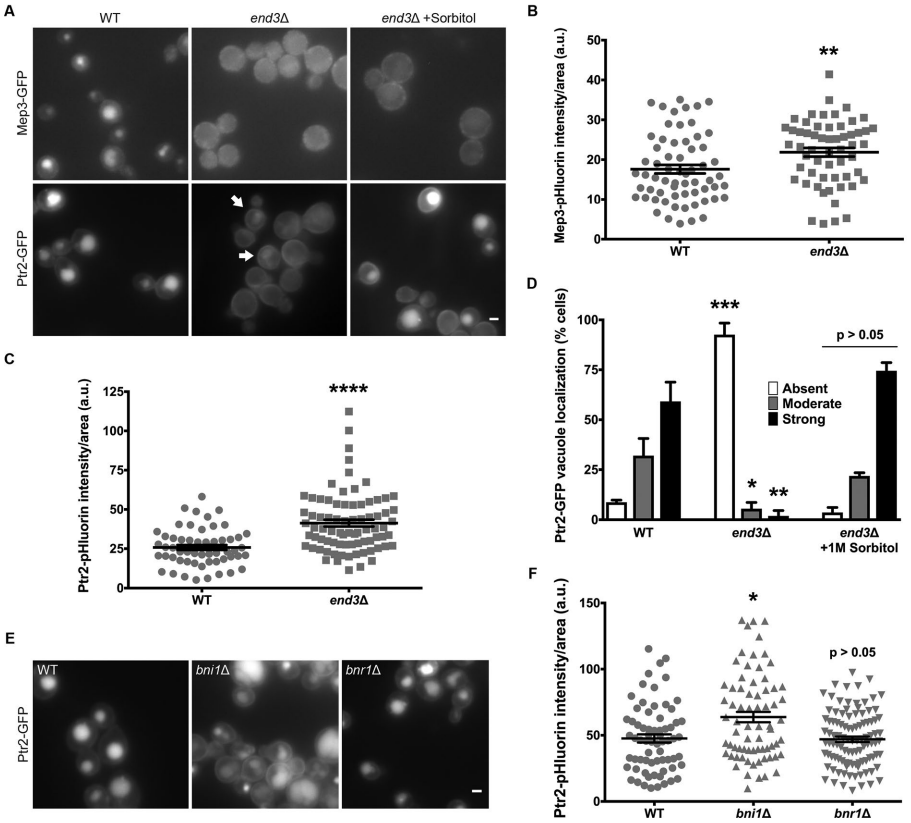

FIGURE 6: Ptr2 can be trafficked via clathrin-independent endocytosis. (A) Cells expressing Mep3-GFP or Ptr2-GFP and lacking End3 were grown on rich medium alongside WT strains in the absence or presence of osmotic support (1 M sorbitol) and imaged by fluorescence microscopy. Arrows indicate cells with internalized Ptr2-GFP. Scale bar, 2 μm. (B) Intensity of Mep3-pHluorin was quantified; intensity values were corrected for cell size and expressed in arbitrary units (a.u.). Error bars indicate mean ± SEM; $^{**}p < 0.01$ compared with WT. (C) Intensity of Ptr2-pHluorin was quantified; intensity values were corrected for cell size and expressed in arbitrary units (a.u.). Error bars indicate mean ± SEM; $^{****}p < 0.0001$ compared with WT. (D) For each condition, Ptr2-GFP–expressing cells were quantified as having a strong, moderate, or weak/absent vacuolar signal, and the percentage in each category was plotted. Error bars indicate mean ± SD; $n = 2$; $^{*}p < 0.05$, $^{**}p < 0.01$, $^{***}p < 0.001$ compared with WT. (E) WT, *bni1*Δ, and *bnr1*Δ cells expressing Ptr2-GFP were grown on rich medium and imaged by fluorescence microscopy. Scale bar, 2 μm. (F) Intensity of Ptr2-pHluorin was quantified for each condition; intensity values were corrected for cell size and expressed in arbitrary units (a.u.). Error bars indicate mean ± SEM; $^{*}p < 0.05$ compared with WT.

This result was encouraging, but the role of End3 in Rho1-dependent CIE has not yet been assessed. To address this, we expressed high-copy *ROM1*, a guanine nucleotide exchange factor for Rho1 that was shown to activate this CIE pathway in CME-deficient cells (Prosser *et al.*, 2011). High-copy *ROM1* decreased the concentration of Ptr2 at the PM in *end3*Δ cells (Supplemental Figure S5, D and E), indicating that End3 is not involved in Rho1-dependent CIE.

Despite the rescue of Ptr2 trafficking from the PM with Rom1 overexpression, vacuoles were not visible in many of the cells. We postulated that this might be due to the outpacing of GFP degradation within the vacuole by the trafficking of Ptr2 to this compartment. To test this, we repeated the experiment with the addition of protease inhibitors to the growth medium. In the presence of protease inhibitors, the vacuoles of *end3*Δ cells expressing high-copy *ROM1* became visible (Supplemental Figure S5F). However, many of the CME mutants possessing the empty vector exhibited no vacuolar fluorescence, similar to untreated cells (Figure 6A; bottom, middle), indicating that treatment with protease inhibitors does not induce vacuolar autofluorescence. This result supports the conclusion that decreased levels of Ptr2 at the PM in CME mutant cells are due to enhanced Rho1-dependent CIE.

To further investigate a role for CIE in Ptr2 trafficking, we constructed *bni1*Δ strains expressing either GFP- or pHluorin-tagged Ptr2. Bni1 is a yeast formin that promotes elongation of linear actin filaments and is required for this CIE pathway (Pruyne *et al.*, 2002; Prosser *et al.*, 2011). In the absence of Bni1, fluorescently tagged Ptr2 accumulated at the PM to a greater extent than in WT cells (Figure 6, E and F). In contrast, cells lacking Bnr1, the second yeast formin, which is not involved in CIE (Prosser *et al.*, 2011), showed localization of Ptr2 chimeras that was indistinguishable from that for WT cells. Therefore the accumulation of Ptr2 at the PM in a *bni1*Δ strain is not a result of altered actin regulation but is instead due to the loss of Rho1-dependent CIE. These data suggest that this CIE pathway contributes observably to Ptr2 internalization in WT cells under standard conditions.

Syp1 contributes to internalization of Ptr2 via Rho1-dependent CIE in addition to CME

On the basis of our observation that Ptr2 can internalize via Rho1-dependent CIE, we sought to determine whether Syp1 mediates trafficking of Ptr2 via this pathway by functioning in the Rho1-dependent CIE pathway. We introduced a high-copy plasmid containing *SYP1* into *end3*Δ cells expressing fluorescently tagged Ptr2 to test whether Syp1 overexpression can rescue Ptr2 endocytosis in this CME-deficient strain. Cells lacking End3 and possessing an empty vector exhibited high levels of Ptr2 at the plasma membrane, as expected. However, in the *end3*Δ strain transformed with high-copy *SYP1*, a significant decrease in the amount of Ptr2 at the PM was observed (Figure 7, A and B). Ptr2 concentration within buds appeared diminished compared with mother cells, and we also noted that the buds often appeared elongated with Syp1 overexpression.

Vacuoles were not visible in many *end3*Δ cells with high-copy *SYP1*, as was observed in similar experiments with Rom1 overexpression (Supplemental Figure S5D). However, addition of protease inhibitors to the growth medium allowed the vacuoles of cells with high-copy *SYP1* to be observed (Supplemental Figure S5F). The results of this experiment support the conclusion that decreases in Ptr2 levels at the PM in these studies are indeed the result of upregulated cargo trafficking into the cell.

To confirm that high-copy *SYP1* restores Ptr2 endocytosis in *end3*Δ cells via CIE and not by rescuing CME, we investigated the effect of high-copy *SYP1* on actin patches associated with CME; previous experiments showed that cortical actin patches are larger and

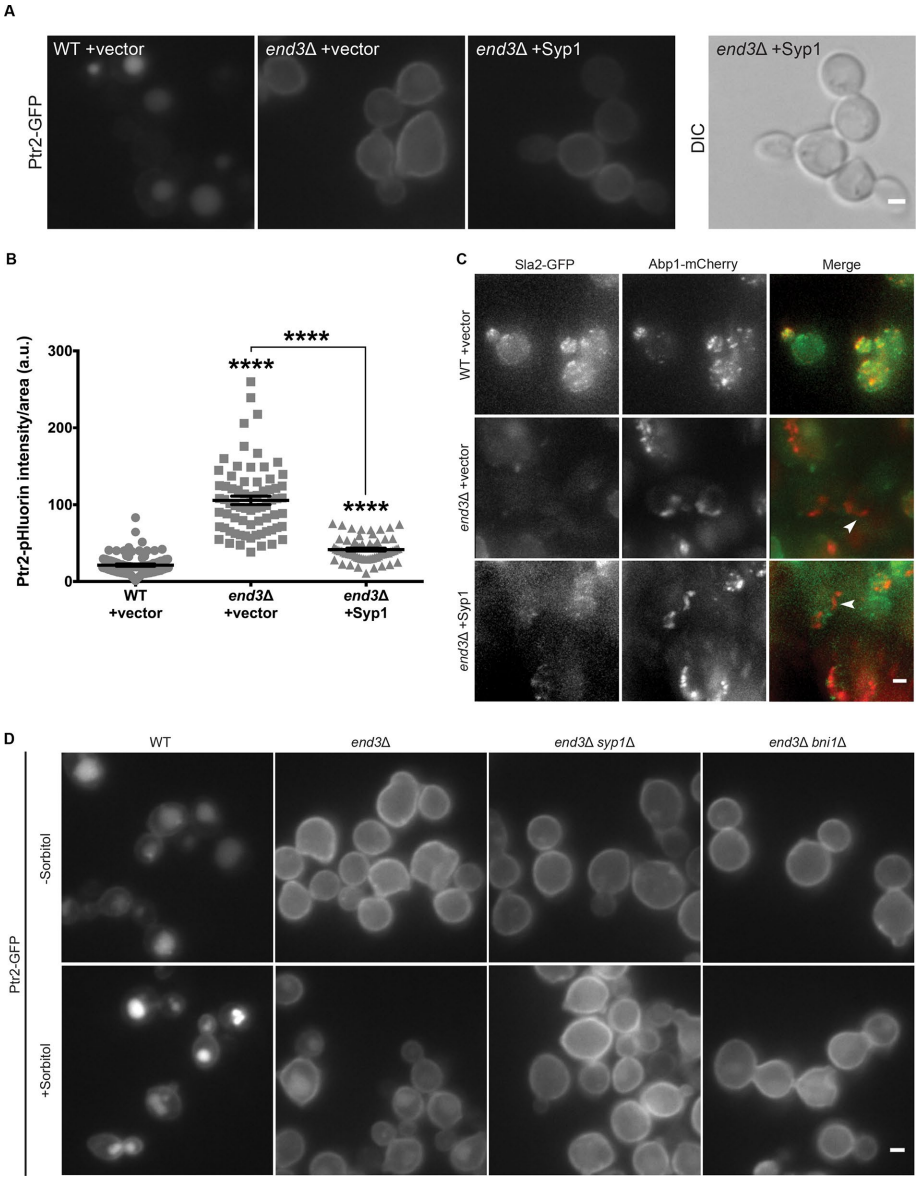

FIGURE 7: Syp1-mediated internalization of Ptr2 occurs via CIE in addition to CME. (A) WT and *end3*Δ cells expressing Ptr2-GFP were transformed with either an empty or *SYP1*-containing high-copy vector and imaged via live-cell fluorescence microscopy. Scale bar, 2 μm. (B) Intensity of Ptr2-pHluorin was quantified for each condition; intensity values were corrected for cell size and expressed in arbitrary units (a.u.). Error bars indicate mean ± SEM; ****$p < 0.0001$ compared with WT. (C) WT and *end3*Δ cells expressing Sla2-GFP and Abp1-mCherry were transformed with either an empty or *SYP1*-containing high-copy vector and imaged via live-cell fluorescence microscopy. Maximum intensity projection images generated from *Z*-stacks. Scale bar, 2 μm. (D) Cells expressing Ptr2-GFP in WT, *end3*Δ, *end3*Δ *syp1*Δ, or *end3*Δ *bni1*Δ strains were grown on rich medium in the presence or absence of 1 M sorbitol and imaged by fluorescence microscopy. Scale bar, 2 μm.

fewer in *end3*Δ cells (Bénédetti *et al.*, 1994). We examined *end3*Δ cells expressing a GFP-tagged CME protein, Sla2, as well as Abp1-mCherry, an F-actin–binding protein that marks actin patches, in the presence and absence of high-copy *SYP1*. As previously reported, actin patches in *end3*Δ cells with empty vector appeared to be larger and fewer in number compared with those in a WT strain (Figure 7C), as well as less dynamic (Supplemental Videos S1–S3). Structures similar to actin comet tails, which are observed in many endocytic mutants (Kaksonen *et al.*, 2005; Newpher and Lemmon, 2006; Prosser *et al.*, 2011; Bradford *et al.*, 2015), were also seen in the absence of End3, and these mutant phenotypes were not rescued by high-copy *SYP1* (Figure 7C, arrowheads, and Supplemental Videos S2 and S3).

We also tested the ability of osmotic support to rescue Ptr2 endocytosis in an *end3*Δ strain lacking functional Rho1-dependent CIE. Ptr2 internalization in an *end3*Δ strain was improved by the addition of sorbitol to the growth medium (Figure 7D), as shown earlier (Figure 6A). However, this enhanced trafficking was largely abolished in an *end3*Δ *bni1*Δ double mutant that is deficient in both CME and CIE. In addition, we observed that high osmolarity was unable to improve Ptr2 internalization in an *end3*Δ *syp1*Δ strain, further suggesting that Ptr2 trafficking via both pathways is Syp1 dependent. Together these results indicate that Syp1 functions in Rho1-dependent CIE and can direct Ptr2 internalization via this pathway.

DISCUSSION

A role for cargo-sorting DxY motifs in endocytosis

DxY motifs appear to be a common feature of Syp1 cargoes, important for recognition and trafficking into the cell; however, DxY was not the most abundant motif present in the phage display peptides. We anticipated the presence of clues regarding the mechanism of physical interaction between Syp1 and its higher-affinity binding partners such as Ede1, which also binds to the region of Syp1 used in the phage display screen (Reider *et al.*, 2009). The large number of WW sequences may be one such indicator, pointing to a separate mechanism dependent on a hydrophobic interaction.

Syp1 may also recognize similar sequences, such as ExY or DxΦ, although we have not yet tested roles for these variants. All of the candidate cargoes that do not possess a DxY motif have a biochemically similar sequence, most of which reside within a predicted cytoplasmic region of the protein. The Snc1$^{63\text{-}93}$ fragment, which binds Syp1 but does not include a DxY motif, contains a DxΦ sequence, DxL (aa 65–67; Figure 2A). This offers a potential recognition site for Syp1. This Snc1 fragment also contains a YxxΦ motif. However, it is unlikely that this motif mediates the interaction between the μHD and this portion of Snc1, because a mutation that disrupted the Snc1 YxxΦ motif still bound efficiently to the Syp1 μHD (Fig S1C).

Mep3 exhibited condition-dependent endocytic trafficking, and the mechanisms underlying precise regulation of cargo internalization in changing growth conditions will be an important area of future research. PhosphoGRID data indicate that the DxY motif in Ptr2, DSY (aa 35–37), can be phosphorylated on both S and Y residues, presenting the possibility that phosphoregulation

mediates uptake of this cargo (Stark *et al.*, 2010); controlled trafficking of protein cargoes by the μ subunit of AP-2 has been observed in mammalian cells (Rapetti-Mauss *et al.*, 2013).

The ability of mammalian Syp1 orthologues to recognize DxY motifs has not been tested. The Mep3 and Ptr2 orthologues RhAG and PepT1, respectively, do not contain DxY motifs but do have DxΦ motifs; it will be interesting to see whether similar interactions between these transporters and FCHo1/2 or SGIP1 occur in mammalian cells. DxΦ sequences are also present in the Ptr2-related protein PepT2, which possesses a DxY motif as well (aa 217–219), and in the FCHo1 cargo Alk8.

Although this study focused on the role of DxY motifs in cargo sorting, biochemically similar sequences also appear to be important for interactions between components of the endocytic machinery. In addition to their role in cargo sorting, DPF motifs are also present in many endocytic proteins, such as Eps15, auxilin, amphiphysin, AP180/PICALM, synaptojanin, and HIP1 (Owen *et al.*, 1999). Recent investigations have demonstrated that the μHD of FCHo1 binds consecutive DPF motifs in Eps15, the homologous domain of FCHo2 interacts with DPF motifs in Dab2, and the μHD of SGIP1 binds successive DPF motifs (Mulkearns and Cooper, 2012; Ma *et al.*, 2016; Shimada *et al.*, 2016). Taken together, these results suggest that DxY and/or DxΦ motifs may play a ubiquitous role in muniscin–cargo interactions.

Future studies will aim to identify further cargo-sorting motifs recognized by muniscins and pinpoint their potentially separate cargo-binding sites, as well as reveal additional cargoes of these adaptors.

Trafficking of Snc1 and its mammalian orthologue, VAMP2 (synaptobrevin)

The large number of adaptor proteins that are known to participate in SNARE endocytosis highlights the importance of SNARE regulation in maintaining cellular physiology (Maritzen *et al.*, 2012). Syp1 is the first adaptor protein observed to bind Snc1 at two sites (Figure 2, D and E), one within and one outside of the SNARE motif, leading to the prediction that Syp1 plays a unique role in Snc1 internalization. $Snc1^{1\text{-}27}$ is predicted to be unstructured (Strop *et al.*, 2008).

Binding of adaptor proteins to the SNARE motif of SNAREs, which is primarily reserved for association with the other SNARE-complex members (e.g., syntaxin/SNAP-25 in mammals), was once believed to be uncommon (Sutton *et al.*, 1998). Two reports revealed that this is not as unusual as originally believed: both CALM and AP180 were shown to traffic and interact with several VAMP family proteins through direct interaction of the AP180/CALM ANTH domain with the N-terminal half of the SNARE motif (Koo *et al.*, 2011; Miller *et al.*, 2011). Together with our data, these results suggest a novel mechanism of SNARE motif–dependent endocytic sorting.

Because Syp1 and the other SNARE motif–binding adaptors associate with v-SNAREs at the sites of SNARE–SNARE interaction, it is likely that NSF-mediated disassembly of *cis*-SNARE complexes will be a prerequisite for Syp1 and AP180/CALM-mediated endocytic recycling of Snc1 and the VAMPs and that the SNARE-motif binding site becomes accessible to Syp1 only after NSF-mediated dissociation. However, Syp1 also binds to a region outside of the SNARE motif, making the range of Syp1–Snc1 interactions an interesting subject of future research.

Identifying additional cargoes of Syp1

Approximately 5% of proteins tested in the visual screen were identified as candidate Syp1 cargoes, and only 1% were successfully confirmed as bona fide cargoes of this adaptor after testing the Syp1 dependence of candidates in multiple genetic backgrounds. It is likely that additional Syp1 cargoes exist that were not detected using this approach, potentially including candidates that did not appear to be true cargo proteins upon validation of results from the visual screen.

There are many possibilities as to why only a fraction of the tested proteins appeared to exhibit Syp1-dependent localization. One is redundancy in cargo protein recognition by other endocytic adaptors, which might become increasingly common when the preferred adaptor is absent and cargo concentration at the PM begins to increase. Moreover, ubiquitination is a major signal for cargo internalization in yeast, and binding of Epsin/AP180 proteins, which are the primary endocytic adaptors in yeast, occurs largely via recognition of ubiquitinated targets (Polo *et al.*, 2002; Shih *et al.*, 2002). The absence of Syp1 in combination with other adaptors may reveal additional cargoes.

Alternatively, the findings in one recent study allow for the possibility of sequential binding by FCHo1/2 and other adaptors to explain the lack of complete penetrance of *syp1* mutant cargo trafficking phenotypes (Ma *et al.*, 2016). In addition, a C-terminally tagged protein library was used in this screen; therefore, it is possible that some Syp1 cargoes are unable to support modifications at their C-terminus. Use of newly available N-terminal libraries may reveal further cargo proteins in cases in which a C-terminal GFP tag impedes internalization (Yofe *et al.*, 2016).

Finally, subtle differences in cargo trafficking between WT and *syp1*Δ strains may not be visible using GFP and instead would become apparent only upon pHluorin quantification or overexpression of Syp1, as seen for Mid2 and Snc1 (Reider *et al.*, 2009; Figure 2B). Growth under altered conditions may also affect cellular requirements for the function and localization of a particular cargo, during which Syp1-dependent regulation may become more observable. This was true for Mep3, which exhibited a more pronounced Syp1-dependent internalization on medium containing high levels of ammonium (Figure 5, A and B). Testing a wider range of growth conditions might also reveal roles for Syp1 in endocytosis of other proteins. Similar visual screens for changes in cargo localization might provide analogous information for other adaptors as well.

Role of multiple endocytic pathways in Syp1-mediated cargo internalization

Budding yeast possess a Rho1-dependent CIE pathway (Prosser *et al.*, 2011); however, few cargoes that can be trafficked via this pathway have been identified. In addition, experiments revealing components of the Rho1-dependent CIE machinery have largely relied on overexpression of CIE factors to demonstrate the endocytosis of cargo. This is consistent with these cargoes being preferentially internalized via CME while also possessing the capacity for uptake via CIE.

We observed partial defects in endocytosis of Ptr2 by simply inactivating CIE (Figure 6, E and F), suggesting that Ptr2 is the first known dual cargo, exhibiting a contribution from CIE for its internalization under standard conditions. Thus, Ptr2 may become a powerful tool for future analysis of CIE mechanisms. Although CIE does not appear to contribute to Mep3 endocytosis, it is possible that other Syp1 cargoes behave similarly to Ptr2 and are trafficked via CIE as well. The discovery of additional Syp1 cargoes may shed light not only on the function of Syp1 but also on roles for CIE.

Evidence that Ptr2 is partially internalized via CIE and that high-copy expression of *SYP1* can induce trafficking via this pathway indicates that Syp1 is among the first adaptors linked to both CME and CIE mechanisms. It is possible that Syp1 localizes to two distinct sets of endocytic sites, helping to establish those

corresponding to nascent CME and CIE events. Syp1 may be recruited to sites of CIE via physical interaction with Mid2 when cargoes are signaled for internalization via this pathway. Our results suggesting a role in both pathways indicate that Syp1 may be an important regulator of yeast endocytosis.

MATERIALS AND METHODS

Strains and plasmids

Complete lists of strains and plasmids used in this study are given in Tables 1 and 2, respectively. Strains were constructed using PCR-based genomic integration as described previously (Longtine *et al.*, 1998; Goldstein and McCusker, 1999; Nishimura *et al.*, 2009). For genomic integration of GFP or pHluorin, we designed primers using the F2 and R1 plasmid-specific sequences (Longtine *et al.*, 1998). Transformations were performed according to standard procedures using the lithium acetate method, and integrations were confirmed by colony PCR and/or Western immunoblotting (unpublished data).

Phage display screen

Phage display 12-mer peptide libraries (of random sequence) fused to the N-terminus of pVIII of M13 filamentous phage were used to select peptide ligands for GST-Syp1 μHD. Phage display selection was carried out as described previously (Tonikian *et al.*, 2007).

Protein purification

Proteins were purified as described previously (Reider *et al.*, 2009). In brief, His_6- and GST-tagged proteins were purified from Rosetta cells (Novagen) transformed with plasmids derived from pET28a or pGEX-KG-KAN. Isopropyl-β-D-thiogalactoside at 0.3 mM was used to induce protein expression in these cells, which were then harvested, frozen to –80°C, and resuspended in buffer containing protease inhibitor cocktail (Roche). His_6-tagged protein lysates were immobilized on Talon metal affinity resin (Clontech), and GST-tagged proteins were isolated with glutathione-agarose (Thermo Fisher).

Binding assays

GST-tagged protein lysates were incubated with glutathione-agarose beads (Sigma-Aldrich) for 2 h at 4°C, washed twice with wash buffer (20 mM 4-(2-hydroxyethyl)-1-piperazineethanesulfonic acid–NaOH, 30 mM NaCl, pH 7.6), and mixed with His_6-tagged protein lysates for 2 h at 4°C. After incubation, the immobilized proteins were washed three times with cold wash buffer before SDS–PAGE sample buffer was added. Supernatant and pellet fractions were resolved by SDS–PAGE, transferred to nitrocellulose, and immunoblotted with mouse anti-His_6 antibody (1:5000; Clontech). Blots were then treated with horseradish peroxidase (HRP)–conjugated goat anti-mouse secondary antibodies (1:10,000) before exposure.

Protein binding quantification

AlphaView SA software was used to quantify the results of binding assays. The intensity of bands visualized by immunoblotting was quantified, and the background-corrected averages were compared with that of appropriate GST or GST-μHD protein detected by GelCode Blue staining. Unpaired *t* tests were used to determine statistical significance.

Media and growth conditions

Standard yeast extract/peptone medium with 2% dextrose (YPD) was used for growth of yeast under rich conditions. For ammonium-rich conditions or plasmid maintenance, standard yeast nitrogen base (YNB) medium containing 38 mM ammonium sulfate, 2% dextrose, and appropriate amino acids and nutrients was used. All yeast were grown at 30°C.

Bacteria were grown in Luria–Bertani (LB) supplemented with 50 μg/ml carbenicillin, 30 μg/ml kanamycin, and/or 34 μg/ml chloramphenicol, as appropriate. Materials were from Fisher Scientific or Sigma Chemical Company unless otherwise stated.

Synthetic genetic array

All genetic manipulations for the high-throughput visual screen were performed using synthetic genetic array techniques as previously described (Tong and Boone, 2006; Cohen and Schuldiner, 2011) to allow efficient introduction of various mutant backgrounds (*syp1*Δ and *end3*Δ) into a collection of secretory pathway–localized proteins harboring a transmembrane domain and tagged with GFP at the C-terminus (Huh *et al.*, 2003).

Briefly, using a RoToR colony arrayer (Singer Instruments, United Kingdom) to manipulate libraries in 384-colony high-density formats, haploid strains from opposing mating types, each harboring a different genomic alteration, were mated on YPD plates. Diploid cells were selected on plates containing all selection markers found on both parent haploid strains. Sporulation was then induced by transferring cells to nitrogen-starvation plates for 5 d. Haploid cells containing all desired mutations were selected for by transferring cells to plates containing all selection markers alongside the toxic amino acid derivatives canavanine and thialysine (S-AEC) to select against remaining diploids.

High-throughput fluorescence microscopy

Microscopic screening was performed using an automated microscopy setup as described previously (Breker *et al.*, 2013). Cells were moved from agar plates into liquid 384-well polystyrene growth plates using the RoToR arrayer. Liquid cultures were grown overnight in SD –His medium in a shaking incubator (LiCONiC Instruments) at 30°C. A JANUS liquid handler (PerkinElmer) connected to the incubator was used to backdilute the strains into plates containing the same medium. Plates were then transferred back to the incubator and allowed to grow for 4 h at 30°C to reach logarithmic growth phase.

The liquid handler was then used to transfer strains into glass-bottom, 384-well microscope plates (Matrical Bioscience) coated with concanavalin A (Sigma-Aldrich) to allow cell adhesion. Wells were washed four times in an imaging medium without fluorescence (SD –His –riboflavin –folic acid) to remove floating cells and reach cell monolayer. Plates were then transferred into an automated inverted fluorescence microscopic ScanR system (Olympus) using a swap robotic arm (Hamilton). Imaging of plates was performed in 384-well format using a 60× air lens (numerical aperture [NA] 0.9) in SD –His –riboflavin –folic acid medium. Images were acquired using the GFP (excitation at 490/20 nm, emission at 535/50 nm) channel.

For cases in which protein topology is undetermined, motifs within Syp1 cargoes were assessed for residence in cytoplasmic regions of the protein using the membrane topology prediction software SPOCTOPUS (Viklund *et al.*, 2008; http://octopus.cbr.su.se/).

Live-cell fluorescence microscopy and quantification of fluorescence intensity

Images were acquired and quantified as described previously (Prosser *et al.*, 2010). In brief, images were obtained at 30°C using an inverted microscope (Axiovert 200; Carl Zeiss) equipped with a Sensicam (Cooke), an X-Cite 120 PC fluorescence illumination system, and a 100×/1.4 NA Plan-Apochromat objective lens. Within

Strain	Genotype	Source
W303	*MATα ura3-1 ade2-1 his3-11 leu2,3112 trp1-1 can1-100 ade2::ADE2*	Laboratory strain
BWY3597	*MATα ura3-1 ade2-1 his3-11 leu2,3112 trp1-1 can1-100 ade2::ADE2 Ste3-GFP::KAN*	This study
BWY6376	*MATα ura3-1 ade2-1 his3-11 leu2,3112 trp1-1 can1-100 ade2::ADE2 Ste3-GFP::KAN syp1::HIS3*	This study
BWY6361	*MATα ura3-1 ade2-1 his3-11 leu2,3112 trp1-1 can1-100 ade2::ADE2 Ste3-GFP::KAN end3::NAT*	This study
BWY6002	*MATα ura3-1 ade2-1 his3-11 leu2,3112 trp1-1 can1-100 ade2::ADE2 Ste3-pHluorin::KAN*	This study
BWY6483	*MATα ura3-1 ade2-1 his3-11 leu2,3112 trp1-1 can1-100 ade2::ADE2 Ste3-pHluorin::KAN syp1::HIS3*	This study
BWY6480	*MATα ura3-1 ade2-1 his3-11 leu2,3112 trp1-1 can1-100 ade2::ADE2 Ste3-pHluorin::KAN end3::NAT*	This study
BWY5735	*MATa ura3-1 ade2-1 his3-11 leu2,3112 trp1-1 can1-100 ade2::ADE2 Ptr2-GFP::KAN*	This study
BWY6015	*MATα ura3-1 ade2-1 his3-11 leu2,3112 trp1-1 can1-100 ade2::ADE2 Ptr2-GFP::KAN syp1::HIS3*	This study
BWY6228	*MATα ura3-1 ade2-1 his3-11 leu2,3112 trp1-1 can1-100 ade2::ADE2 Ptr2-pHluorin::KAN*	This study
BWY6229	*MATa ura3-1 ade2-1 his3-11 leu2,3112 trp1-1 can1-100 ade2::ADE2 Ptr2-pHluorin::KAN syp1::HIS3*	This study
BWY6329	*MATα ura3-1 ade2-1 his3-11 leu2,3112 trp1-1 can1-100 ade2::ADE2 Mep3-GFP::KAN*	This study
BWY5744	*MATa ura3-1 ade2-1 his3-11 leu2,3112 trp1-1 can1-100 ade2::ADE2 Mep3-GFP::KAN syp1::HIS3*	This study
BWY6371	*MATa ura3-1 ade2-1 his3-11 leu2,3112 trp1-1 can1-100 ade2::ADE2 Mep3-pHluorin::KAN*	This study
BWY6375	*MATα ura3-1 ade2-1 his3-11 leu2,3112 trp1-1 can1-100 ade2::ADE2 Mep3-pHluorin::KAN syp1::HIS3*	This study
BWY5739	*MATa ura3-1 ade2-1 his3-11 leu2,3112 trp1-1 can1-100 ade2::ADE2 Arn1-GFP::KAN*	This study
BWY5740	*MATa ura3-1 ade2-1 his3-11 leu2,3112 trp1-1 can1-100 ade2::ADE2 Arn1-GFP::KAN syp1::HIS3*	This study
BWY5733	*MATa ura3-1 ade2-1 his3-11 leu2,3112 trp1-1 can1-100 ade2::ADE2 Csh1-GFP::KAN*	This study
BWY5734	*MATα ura3-1 ade2-1 his3-11 leu2,3112 trp1-1 can1-100 ade2::ADE2 Csh1-GFP::KAN syp1::HIS3*	This study
BWY5729	*MATa ura3-1 ade2-1 his3-11 leu2,3112 trp1-1 can1-100 ade2::ADE2 Hip1-GFP::KAN*	This study
BWY5730	*MATa ura3-1 ade2-1 his3-11 leu2,3112 trp1-1 can1-100 ade2::ADE2 Hip1-GFP::KAN syp1::HIS3*	This study
BWY6380	*MATα ura3-1 ade2-1 his3-11 leu2,3112 trp1-1 can1-100 ade2::ADE2 Mep2-GFP::KAN*	This study
BWY6370	*MATα ura3-1 ade2-1 his3-11 leu2,3112 trp1-1 can1-100 ade2::ADE2 Mep2-GFP::KAN syp1::HIS3*	This study
BWY5737	*MATa ura3-1 ade2-1 his3-11 leu2,3112 trp1-1 can1-100 ade2::ADE2 Mrh1-GFP::KAN*	This study
BWY5738	*MATa ura3-1 ade2-1 his3-11 leu2,3112 trp1-1 can1-100 ade2::ADE2 Mrh1-GFP::KAN syp1::HIS3*	This study
BWY5745	*MATa ura3-1 ade2-1 his3-11 leu2,3112 trp1-1 can1-100 ade2::ADE2 Pex22-GFP::KAN*	This study
BWY5746	*MATa ura3-1 ade2-1 his3-11 leu2,3112 trp1-1 can1-100 ade2::ADE2 Pex22-GFP::KAN syp1::HIS3*	This study
BWY5741	*MATa ura3-1 ade2-1 his3-11 leu2,3112 trp1-1 can1-100 ade2::ADE2 Sit1-GFP::KAN*	This study
BWY5742	*MATα ura3-1 ade2-1 his3-11 leu2,3112 trp1-1 can1-100 ade2::ADE2 Sit1-GFP::KAN syp1::HIS3*	This study
BWY6434	*MATa ura3-1 ade2-1 his3-11 leu2,3112 trp1-1 can1-100 ade2::ADE2 Ykl077w-GFP::KAN*	This study
BWY6435	*MATα ura3-1 ade2-1 his3-11 leu2,3112 trp1-1 can1-100 ade2::ADE2 Ykl077w-GFP::KAN syp1::HIS3*	This study
BWY6227	*MATα ura3-1 ade2-1 his3-11 leu2,3112 trp1-1 can1-100 ade2::ADE2 mep3(aa1-430)-GFP::KAN*	This study
BWY6757	*MATa ura3-1 ade2-1 his3-11 leu2,3112 trp1-1 can1-100 ade2::ADE2 mep3(aa1-433)-GFP::KAN*	This study
BWY6908	*MATα ura3-1 ade2-1 his3-11 leu2,3112 trp1-1 can1-100 ade2::ADE2 mep3(aa1-433)-GFP::KAN syp1::HIS3*	This study
BWY6226	*MATα ura3-1 ade2-1 his3-11 leu2,3112 trp1-1 can1-100 ade2::ADE2 mep3(aa1-430)-pHluorin::KAN*	This study
BWY6758	*MATa ura3-1 ade2-1 his3-11 leu2,3112 trp1-1 can1-100 ade2::ADE2 mep3(aa1-433)-pHluorin::KAN*	This study
BWY6910	*MATa ura3-1 ade2-1 his3-11 leu2,3112 trp1-1 can1-100 ade2::ADE2 mep3(aa1-433)-pHluorin::KAN syp1::HIS3*	This study
BWY2919	*MATa ura3-1 ade2-1 his3-11 leu2,3112 trp1-1 can1-100 ade2::ADE2 Mid2-GFP::KAN*	Reider *et al*. (2009)
BWY6755	*MATa ura3-1 ade2-1 his3-11 leu2,3112 trp1-1 can1-100 ade2::ADE2 mid2(aa1-286)-GFP::KAN*	This study
BWY6756	*MATa ura3-1 ade2-1 his3-11 leu2,3112 trp1-1 can1-100 ade2::ADE2 mid2(aa1-289)-GFP::KAN*	This study
BWY3893	*MATα ura3-1 ade2-1 his3-11 leu2,3112 trp1-1 can1-100 ade2::ADE2 Syp1-GFP::KAN*	Reider *et al*. (2009)
BWY3210	*MATα ura3-1 ade2-1 his3-11 leu2,3112 trp1-1 can1-100 ade2::ADE2 Ede1-GFP::KAN*	Reider *et al*. (2009)

TABLE 1: Strains used in this study.

Continues

Strain	Genotype	Source
BWY6368	*MATα ura3-1 ade2-1 his3-11 leu2,3112 trp1-1 can1-100 ade2::ADE2 Mep3-GFP::KAN end3::NAT*	This study
BWY6396	*MATa ura3-1 ade2-1 his3-11 leu2,3112 trp1-1 can1-100 ade2::ADE2 Mep3-pHluorin::KAN end3::NAT*	This study
BWY6363	*MATa ura3-1 ade2-1 his3-11 leu2,3112 trp1-1 can1-100 ade2::ADE2 Ptr2-GFP::KAN end3::NAT*	This study
BWY6366	*MATα ura3-1 ade2-1 his3-11 leu2,3112 trp1-1 can1-100 ade2::ADE2 Ptr2-pHluorin::KAN end3::NAT*	This study
BWY6254	*MATa ura3-1 ade2-1 his3-11 leu2,3112 trp1-1 can1-100 ade2::ADE2 Ptr2-GFP::KAN bni1::NAT*	This study
BWY6387	*MATa ura3-1 ade2-1 his3-11 leu2,3112 trp1-1 can1-100 ade2::ADE2 Ptr2-GFP::KAN bnr1::NAT*	This study
BWY6388	*MATα ura3-1 ade2-1 his3-11 leu2,3112 trp1-1 can1-100 ade2::ADE2 Ptr2-pHluorin::KAN bni1::NAT*	This study
BWY6391	*MATa ura3-1 ade2-1 his3-11 leu2,3112 trp1-1 can1-100 ade2::ADE2 Ptr2-pHluorin::KAN bnr1::NAT*	This study
BWY6378	*MATa ura3-1 ade2-1 his3-11 leu2,3112 trp1-1 can1-100 ade2::ADE2 Mid2-GFP::KAN end3::NAT*	This study
BWY6781	*MATα ura3-1 ade2-1 his3-11 leu2,3112 trp1-1 can1-100 ade2::ADE2 Sla2-GFP::KAN Abp1-mCherry::HPH*	This study
BWY6782	*MATα ura3-1 ade2-1 his3-11 leu2,3112 trp1-1 can1-100 ade2::ADE2 Sla2-GFP::KAN Abp1-mCherry::HPH end3::NAT*	This study
BWY6386	*MATα ura3-1 ade2-1 his3-11 leu2,3112 trp1-1 can1-100 ade2::ADE2 Ptr2-GFP::KAN end3::NAT syp1::HIS3*	This study
BWY6426	*MATα ura3-1 ade2-1 his3-11 leu2,3112 trp1-1 can1-100 ade2::ADE2 Ptr2-GFP::KAN end3::NAT bni1::NAT*	This study

TABLE 1: Strains used in this study. Continued

an experiment, images were acquired using identical exposure conditions; subsequently brightness and contrast adjustments were applied equally to all images.

For quantification of fluorescence intensity, background subtraction was performed using ImageJ, and integrated density was measured for a minimum of 50 cells per condition. All integrated density values were then corrected for cell size. Fluorescence intensity measurements were performed for all cells in a minimum of two separate fields per experimental group. Statistical analysis was performed using Prism (GraphPad); either Welch's unequal-variances *t* test or one-way analysis of variance with Tukey's correction was used.

When use of pHluorin was precluded, trafficking of GFP-tagged protein into cells was assessed via blind quantification of the percentage of cells in each experimental group with one of three

Plasmid	Details	Source
pBW1546	pGEX-KG-KAN	Reider *et al*. (2009)
pBW1503	pGEX-KG-KAN::*Syp1*(aa602-870)	Reider *et al*. (2009)
pBW2250	pET28aC/U::*Mid2*(aa273-376)	This study
pBW2505	pET28aC/U::*mid2*(aa273-376; W277A, Y278A)	This study
pBW2515	pET28aC/U::*mid2*(aa273-376; D14A, E15A, Y16A)	This study
pBW2019	pRS316::*GFP-Snc1*	Quenneville *et al*. (2006)
pRS425	2μ, *LEU2*	Laboratory plasmid
pBW1034	pRS425::*SYP1* (2μ, *LEU2*)	This study
pBW1916	pET28aC/U::*Snc1*(aa1-93)	This study
pBW2326	pET28aC/U::*Snc1*(aa1-27)	This study
pBW2336	pET28aC/U::*snc1*(aa1-27; D8A, P9A, Y10A)	This study
pBW1973	pET28aC/U::*snc1*(aa1-93; D8K, Y10A)	This study
pBW2330	pET28aC/U::*Snc1*(aa63-93)	This study
pBW2439	pET28aC/U::*snc1*(aa63-93; W86A, Y87A)	This study
pRS426	2μ, *URA3*	Laboratory plasmid
pBW1446	pRS426::*Syp1* (2μ, *URA3*)	Reider *et al*. (2009)
pBW1562	pRS426::*Syp1* (aa1-601) (2μ, *URA3*)	Reider *et al*. (2009)
pBW1622	pYEP352::*Rom1* (2μ, URA3)	Ozaki *et al*. (1996)

TABLE 2: Plasmids used in this study.

vacuolar fluorescence phenotypes; at least 50 cells per condition per replicate were categorized as having either a weak/absent, moderate, or strong fluorescence signal at the vacuole. Unpaired *t* tests of all replicates were then performed, comparing each experimental phenotypic class to its respective WT class at the same time point.

Z-stacks were acquired for maximum intensity projections using 0.25-µm step intervals. Projections were generated using ImageJ.

LatA treatment

Cells were grown to logarithmic phase and resuspended in synthetic medium containing 200 µM LatA (Invitrogen) or an equivalent volume of dimethyl sulfoxide. Cells were incubated for 2 h at 30°C before imaging to allow for protein accumulation at the plasma membrane.

Urea extraction and trichloroacetic acid precipitation

For urea extraction of membrane proteins, 5 OD of mid log-phase cells expressing Ptr2-GFP or Mep3-GFP were grown in rich or ammonium-rich medium, respectively, collected, and washed with 1 ml of phosphate-buffered saline. Cells were then vortexed for 90 s with 100 µl of acid-washed glass 0.5-mm beads and 100 µl of 1× Laemmli urea sample buffer and incubated at room temperature for 5 min before analysis.

For trichloroacetic acid (TCA) precipitation of soluble proteins, 5 OD of mid log-phase cells expressing Syp1-GFP were grown in rich and ammonium-rich media, collected, and resuspended in 1 ml of 10% TCA. Cells were incubated on ice for 20 min and then pelleted at 14,000 rpm for 10 min at 4°C. The pellets were washed twice with cold acetone, dried, and resuspended in SDS sample buffer. Samples were then heated to 65°C for 5 min before analysis.

Samples were resolved by SDS–PAGE, transferred to nitrocellulose, and immunoblotted with mouse anti-GFP antibody (1:2000; Santa Cruz Biotechnology) and HRP-conjugated goat anti-mouse secondary antibodies (1:5000) before exposure.

Growth assays

Growth curves were generated using a Tecan Infinite M200 plate reader. WT or *syp1*Δ cultures were grown in YNB medium with or without methylammonium in 24-well, flat-bottom tissue culture plates (Corning). Cultures were adjusted to equivalent starting density and volume and then grown at 30°C with shaking, with the OD_{600} for each condition measured every 30 min for 16 h.

ACKNOWLEDGMENTS

We thank Nate Snyder for help with this work during a rotation in the Wendland lab, as well as the labs of M. Andrew Hoyt and Kyle Cunningham for the generous sharing of equipment and reagents. We are also grateful to Dalia Elinger for performing the genetic crosses required for the Syp1 cargo screen, Michael McCaffery and staff of the Johns Hopkins University Integrated Imaging Center, and members of the Wendland lab for immensely helpful discussions and suggestions. This work was funded by Grant RO1 GM60979 from the National Institutes of Health to B.W. and a Minerva Grant to M.S. K.H. and A.R.A. were supported in part by a National Institutes of Health T32 Training Grant (T32 007231-37).

REFERENCES

Ayscough KR, Stryker J, Pokala N, Sanders M, Crews P, Drubin DG (1997). High rates of actin filament turnover in budding yeast and roles for actin in establishment and maintenance of cell polarity revealed using the actin inhibitor latrunculin-A. J Cell Biol 137, 399–416.

Bénédetti H, Raths S, Crausaz F, Riezman H (1994). The END3 gene encodes a protein that is required for the internalization step of endocytosis and for actin cytoskeleton organization in yeast. Mol Biol Cell 5, 1023–1037.

Boettner DR, D'Agostino JL, Torres OT, Daugherty-Clarke K, Uygur A, Reider A, Wendland B, Lemmon SK, Goode BL (2009). The F-BAR protein Syp1 negatively regulates WASp-Arp2/3 complex activity during endocytic patch formation. Curr Biol 19, 1979–1987.

Boll W, Ohno H, Songyang Z, Rapoport I, Cantley LC, Bonifacino JS, Kirchhausen T (1996). Sequence requirements for the recognition of tyrosine-based endocytic signals by clathrin AP-2 complexes. EMBO J 15, 5789–5795.

Bradford MK, Whitworth K, Wendland B (2015). Pan1 regulates transitions between stages of clathrin-mediated endocytosis. Mol Biol Cell 26, 1371–1385.

Breker M, Gymrek M, Schuldiner M (2013). A novel single-cell screening platform reveals proteome plasticity during yeast stress responses. J Cell Biol 200, 839–850.

Burston HE, Maldonado-Baez L, Davey M, Montpetit B, Schluter C, Wendland B, Conibear E (2009). Regulators of yeast endocytosis identified by systematic quantitative analysis. J Cell Biol 185, 1097–1110.

Chapa-y-Lazo B, Allwood EG, Smaczynska-de Rooij II, Snape ML, Ayscough KR (2014). Yeast endocytic adaptor AP-2 binds the stress sensor Mid2 and functions in polarized cell responses. Commun Integr Biol eCollection 7, e2852210.4161/cib.28522.

Cohen Y, Schuldiner M (2011). Advanced methods for high-throughput microscopy screening of genetically modified yeast libraries. Methods Mol Biol 781, 127–159.

Conrad M, Schothorst J, Kankipati HN, Van Zeebroeck G, Rubio-Texeira M, Thevelein JM (2014). Nutrient sensing and signaling in the yeast Saccharomyces cerevisiae. FEMS Microbiol Rev 38, 254–299.

Davis NG, Horecka JL, Sprague GF Jr (1993). Cis- and trans-acting functions required for endocytosis of the yeast pheromone receptors. J Cell Biol 122, 53–65.

Doray B, Lee I, Knisely J, Bu GJ, Kornfeld S (2007). The gamma/sigma 1 and alpha/sigma 2 hemicomplexes of clathrin adaptors AP-1 and AP-2 harbor the dileucine recognition site. Mol Biol Cell 18, 1887–1896.

Engqvist-Goldstein AEY, Drubin DG (2003). Actin assembly and endocytosis: from yeast to mammals. Annu Rev Cell Dev Biol 19, 287–332.

Goldstein AL, McCusker JH (1999). Three new dominant drug resistance cassettes for gene disruption in Saccharomyces cerevisiae. Yeast 15, 1541–1553.

Goode BL, Eskin JA, Wendland B (2015). Actin and endocytosis in budding yeast. Genetics 199, 315–358.

Gurunathan S, Chapman-Shimshoni D, Trajkovic S, Gerst JE (2000). Yeast exocytic v-SNAREs confer endocytosis. Mol Biol Cell 11, 3629–3643.

Hauser M, Kauffman S, Naider F, Becker JM (2005). Substrate preference is altered by mutations in the fifth transmembrane domain of Ptr2p, the di/tri-peptide transporter of Saccharomyces cerevisiae. Mol Mem Biol 22, 215–227.

Heitman J, Agre P (2000). A new face of the Rhesus antigen. Nat Genet 26, 258–259.

Henne WM, Boucrot E, Meinecke M, Evergren E, Vallis Y, Mittal R, McMahon HT (2010). FCHo proteins are nucleators of clathrin-mediated endocytosis. Science 328, 1281–1284.

Howard JP, Hutton JL, Olson JM, Payne GS (2002). Sla1p serves as the targeting signal recognition factor for NPFX(1,2)D-mediated endocytosis. J Cell Biol 157, 315–326.

Huang C, Chang A (2011). pH-dependent cargo sorting from the Golgi. J Biol Chem 286, 10058–10065.

Huh WK, Falvo JV, Gerke LC, Carroll AS, Howson RW, Weissman JS, O'Shea EK (2003). Global analysis of protein localization in budding yeast. Nature 425, 686–691.

Jain RK, Joyce PB, Molinete M, Halban PA, Gorr SU (2001). Oligomerization of green fluorescent protein in the secretory pathway of endocrine cells. Biochem J 360, 645–649.

Kaksonen M, Sun Y, Drubin DG (2003). A pathway for association of receptors, adaptors, and actin during endocytic internalization. Cell 115, 475–87.

Kaksonen M, Toret CP, Drubin DG (2005). A modular design for the clathrin- and actin-mediated endocytosis machinery. Cell 123, 305–320.

Kelly BT, McCoy AJ, Spate K, Miller SE, Evans PR, Honing S, Owen DJ (2008). A structural explanation for the binding of endocytic dileucine motifs by the AP2 complex. Nature 456, 976–979.

Keyel PA, Mishra SK, Roth R, Heuser JE, Watkins SC, Traub LM (2006). A single common portal for clathrin-mediated endocytosis of distinct cargo governed by cargo-selective adaptors. Mol Biol Cell 17, 4300–4317.

Koo SJ, Markovic S, Puchkov D, Mahrenholz CC, Beceren-Braun F, Maritzen T, Dernedde J, Volkmer R, Oschkinat H, Haucke V (2011). SNARE motif-mediated sorting of synaptobrevin by the endocytic adaptors clathrin assembly lymphoid myeloid leukemia (CALM) and AP180 at synapses. Proc Natl Acad Sci USA 108, 13540–13545.

Longtine MS, McKenzie A III, Demarini DJ, Shah NG, Wach A, Brachat A, Philippsen P, Pringle JR (1998). Additional modules for versatile and economical PCR-based gene deletion and modification in Saccharomyces cerevisiae. Yeast 14, 953–961.

Ma L, Umasankar PK, Wrobel AG, Lymar A, McCoy AJ, Holkar SS, Jha A, Pradhan-Sundd T, Watkins SC, Owen DJ, Traub LM (2016). Transient Fcho1/2·Eps15/R·AP-2 nanoclusters prime the AP-2 clathrin adaptor for cargo binding. Dev Cell 37, 428–43.

Marini AM, Soussi-Boudekou S, Vissers S, Andre B (1997). A family of ammonium transporters in Saccharomyces cerevisiae. Mol Cell Biol 17, 4282–4293.

Maritzen T, Koo SJ, Haucke V (2012). Turning CALM into excitement: AP180 and CALM in endocytosis and disease. Biol Cell 104, 588–602.

Miesenbock G, De Angelis DA, Rothman JE (1998). Visualizing secretion and synaptic transmission with pH-sensitive green fluorescent proteins. Nature 394, 192–195.

Miller SE, Sahlender DA, Graham SC, Höning S, Robinson MS, Peden AA, Owen DJ (2011). The molecular basis for the endocytosis of small R-SNAREs by the clathrin adaptor CALM. Cell 147, 1118–1131.

Mulkearns EE, Cooper JA (2012). FCH domain only-2 organizes clathrin-coated structures and interacts with Disabled-2 for low-density lipoprotein receptor endocytosis. Mol Biol Cell 23, 1330–1342.

Newpher TM, Lemmon SK (2006). Clathrin is important for normal actin dynamics and progression of Sla2p-containing patches during endocytosis in yeast. Traffic 7, 574–588.

Nishimura K, Fukagawa T, Takisawa H, Kakimoto T, Kanemaki M (2009). An auxin-based degron system for the rapid depletion of proteins in nonplant cells. Nat Methods 6, 917–922.

Owen DJ, Collins BM, Evans PR (2004). Adaptors for clathrin coats: structure and function. Annu Rev Cell Dev Biol 20, 153–191.

Owen DJ, Vallis Y, Noble MEM, Hunter JB, Dafforn TR, Evans PR, McMahon HT (1999). A structural explanation for the binding of multiple ligands by the alphaadaptin appendage domain. Cell 97, 805–815.

Ozaki K, Tanaka K, Imamura H, Hihara T, Kameyama T, Nonaka H, Hirano H, Matsuura Y, Takai Y (1996). Rom1p and Rom2p are GDP/GTP exchange proteins (GEPs) for the Rho1p small GTP binding protein in Saccharomyces cerevisiae. EMBO J 15, 2196–207.

Piao HL, Machado IM, Payne GS (2007). NPFXD-mediated endocytosis is required for polarity and function of a yeast cell wall stress sensor. Mol Biol Cell 18, 57–65.

Polo S, Sigismund S, Faretta M, Guidi M, Capua MR, Bossi G, Chen H, De Camilli P, Di Fiore PP (2002). A single motif responsible for ubiquitin recognition and monoubiquitination in endocytic proteins. Nature 416, 451–455.

Prosser DC, Drivas TG, Maldonado-Báez L, Wendland B (2011). Existence of a novel clathrin-independent endocytic pathway in yeast that depends on Rho1 and formin. J Cell Biol 195, 657–671.

Prosser DC, Whitworth K, Wendland B (2010). Quantitative analysis of endocytosis with cytoplasmic pHluorin chimeras. Traffic 11, 1141–1150.

Prosser DC, Wrasman K, Woodard TK, O'Donnell AF, Wendland B (2016). Applications of pHluorin for quantitative, kinetic and high-throughput analysis of endocytosis in budding yeast. J Vis Exp 116, 10.3791/54587.

Pruyne D, Evangelista M, Yang C, Bi E, Zigmond S, Bretscher A, Boone C (2002). Role of formins in actin assembly: nucleation and barbed-end association. Science 297, 612–615.

Quenneville NR, Chao TY, McCaffery JM, Conibear E (2006). Domains within the GARP subunit Vps54 confer separate functions in complex assembly and early endosome recognition. Mol Biol Cell 17, 1859–1870.

Rapetti-Mauss R, O'Mahony F, Sepulveda FV, Urbach V, Harvey BJ (2013). Oestrogen promotes KCNQ1 potassium channel endocytosis and postendocytic trafficking in colonic epithelium. J Physiol 591, 2813–2831.

Raths S, Rohrer J, Crausaz F, Riezman H (1993). end3 and end4: two mutants defective in receptor-mediated and fluid-phase endocytosis in Saccharomyces cerevisiae. J Cell Biol 120, 55–65.

Reider A, Barker SL, Mishra SK, Im YJ, Maldonado-Baez L, Hurley JH, Traub LM, Wendland B (2009). Syp1 is a conserved endocytic adaptor that contains domains involved in cargo selection and membrane tubulation. EMBO J 28, 3103–3116.

Reider A, Wendland B (2011). Endocytic adaptors–social networking at the plasma membrane. J Cell Sci 124, 1613–1622.

Robinson M, Poon PP, Schindler C, Murray LE, Kama R, Gabriely G, Singer RA, Spang A, Johnston GC, Gerst JE (2006). The Gcs1 Arf-GAP mediates Snc1,2 v-SNARE retrieval to the Golgi in yeast. Mol Biol Cell 17, 1845–1858.

Saier MH Jr (2000). A functional-phylogenetic classification system for transmembrane solute transporters. Microbiol Mol Biol Rev 64, 354–411.

Shih SC, Katzmann DJ, Schnell JD, Sutanto M, Emr SD, Hicke L (2002). Epsins and Vps27p/Hrs contain ubiquitin-binding domains that function in receptor endocytosis. Nat Cell Biol 4, 389–393.

Shimada A, Yamaguchi A, Kohda D (2016). Structural basis for the recognition of two consecutive mutually interacting DPF motifs by the SGIP1 μ homology domain. Sci Rep 6, 19565.

Stark C, Su TC, Breitkreutz A, Lourenco P, Dahabieh M, Breitkreutz BJ, Tyers M, Sadowski I (2010). PhosphoGRID: a database of experimentally verified in vivo protein phosphorylation sites from the budding yeast Saccharomyces cerevisiae. Database (Oxford) 2010, bap026.

Steiner HY, Song W, Zhang L, Naider F, Becker JM, Stacey G (1994). An Arabidopsis peptide transporter is a member of a new class of membrane transport proteins. Plant Cell 6, 1289–1299.

Stimpson HE, Toret CP, Cheng AT, Pauly BS, Drubin DG (2009). Early-arriving Syp1p and Ede1p function in endocytic site placement and formation in budding yeast. Mol Biol Cell 20, 4640–4651.

Strop P, Kaiser SE, Vrljic M, Brunger AT (2008). The structure of the yeast plasma membrane SNARE complex reveals destabilizing water-filled cavities. J Biol Chem 283, 1113–1119.

Sutton RB, Fasshauer D, Jahn R, Brunger AT (1998). Crystal structure of a SNARE complex involved in synaptic exocytosis at 2.4 A resolution. Nature 395, 347–353.

Tang HY, Munn A, Cai M (1997). EH domain proteins Pan1p and End3p are components of a complex that plays a dual role in organization of the cortical actin cytoskeleton and endocytosis in Saccharomyces cerevisiae. Mol Cell Biol 17, 4294–4304.

Tang HY, Xu J, Cai M (2000). Pan1p, End3p, and S1a1p, three yeast proteins required for normal cortical actin cytoskeleton organization, associate with each other and play essential roles in cell wall morphogenesis. Mol Cell Biol 20, 12–25.

Taylor MJ, Perrais D, Merrifield CJ (2011). A high precision survey of the molecular dynamics of mammalian clathrin-mediated endocytosis. PLoS Biol 9, e1000604.

Tong AH, Boone C (2006). Synthetic genetic array analysis in *Saccharomyces cerevisiae*. Methods Mol Biol 313, 171–192.

Tonikian R, Zhang Y, Boone C, Sidhu SS (2007). Identifying specificity profiles for peptide recognition modules from phage-displayed peptide libraries. Nat Protoc 2, 1368–1386.

Traub LM (2009). Tickets to ride: selecting cargo for clathrin-regulated internalization. Nat Rev Mol Cell Biol 10, 583–596.

Umasankar PK, Sanker S, Thieman JR, Chakraborty S, Wendland B, Tsang M, Traub LM (2012). Distinct and separable activities of the endocytic clathrin-coat components Fcho1/2 and AP-2 in developmental patterning. Nat Cell Biol 14, 488–501.

Viklund H, Bernsel A, Skwark M, Elofsson A (2008). SPOCTOPUS: a combined predictor of signal peptides and membrane protein topology. Bioinformatics 24, 2928–2929.

Wegener KL, Partridge AW, Han J, Pickford AR, Liddington RC, Ginsberg MH, Campbell ID (2007). Structural basis of integrin activation by talin. Cell 128, 171–182.

Yofe I, Weill U, Meurer M, Chuartzman S, Zalckvar E, Goldman O, Ben-Dor S, Schütze C, Wiedemann N, Knop M, *et al.* (2016). One library to make them all: streamlining the creation of yeast libraries via a SWAp-Tag strategy. Nat Methods 13, 371–378.